SKOR1 mediates FER kinase-dependent invasive growth of breast cancer cells

SKOR1 mediates FER kinase-dependent invasive growth of breast cancer cells

Lilian M. Sluimer[1], Esme Bullock[2], Max A. K. Rätze[1], Lotte Enserink[1], Celine Overbeeke[1], Marten Hornsveld[3], Valerie G. Brunton[2], Patrick W. B. Derksen[1,*], Sandra Tavares[1,4,5,*]

[1]Department of Pathology, University Medical Center Utrecht, Heidelberglaan 100, 3584 CX Utrecht, The Netherlands
[2]Edinburgh Cancer Research UK Centre, University of Edinburgh, Crewe Road South, EH4 2XR Edinburgh, Scotland, UK
[3]Department of Molecular Cell Biology, Cancer Genomics Centre Netherlands and Centre for Biomedical Genetics, Leiden University Medical Center, Einthovenweg 20, 2333 ZC Leiden, The Netherlands
[4]i3S - Instituto de Investigação e Inovação em Saúde, Universidade do Porto, Rua Alfredo Allen 208, 4200-135 Porto, Portugal
[5]IPATIMUP - Instituto de Patologia e Imunologia Molecular da Universidade do Porto, Rua Júlio Amaral de Carvalho 45, 4200-135 Porto, Portugal

*correspondence:
Sandra Tavares; Rua Alfredo Allen 208, 4200-135 Porto, Portugal; e-mail: stavares@ipatimup.pt
or
Patrick Derksen; Heidelberglaan 100, 3584CX Utrecht, the Netherlands, email: p.w.b.derksen@umcutrecht.nl

Keywords: Breast cancer, FER tyrosine kinase, SKOR1, metastasis, analogue-sensitive, CRISPR-Cas9.

Summary Statement

The SKI FAMILY TRANSCRIPTIONAL COREPRESSOR 1 (SKOR1) has been mainly associated with neuronal development. Now, Sluimer *et al*. identify SKOR1 as a direct substrate of the oncogenic tyrosine kinase FER and a driver of TNBC progression.

Abstract

High expression of the non-receptor tyrosine kinase FER is an independent prognostic factor that correlates with poor survival in breast cancer patients. To investigate whether the kinase activity is essential for FER oncogenic properties, we developed an ATP analogue-sensitive knock-in allele (FER^{ASKI}). Specific FER kinase inhibition in MDA-MB-231 cells reduces migration, invasion, and metastasis in a mouse model of breast cancer. Using the FER^{ASKI} system, we identify SKI family

transcriptional corepressor 1 (SKOR1) as a direct FER kinase substrate. SKOR1 loss phenocopies FER inhibition, leading to impaired proliferation, migration and invasion, and inhibition of breast cancer growth and metastasis formation in mice. We show that the candidate FER phosphorylation residue, SKOR1-Y234, is essential for FER-dependent tumor progression features. Finally, our work suggests that the SKOR1-Y234 residue promotes Smad2/3 signaling through SKOR1 binding to Smad3 attenuation. Our study thus identifies SKOR1 as a mediator of FER-dependent progression of high-risk breast cancers.

List of Abbreviations

FPS/FES-related non-receptor tyrosine kinase (FER)

SKI family transcriptional corepressor 1 (SKOR1)

Triple Negative Breast Cancer (TNBC)

Transforming Growth Factor β (TGFβ)

Bone Morphogenic Protein (BMP)

Sp100/AIRE-1/NucP41/75/DEAF-1 (SAND)

Interaction loop (I-loop)

functional Smad suppressor element on chromosome 15 (Fussel-15)

FER analogue-sensitive (FER-AS)

FER analogue-sensitive knock-in allele (FER^{ASKI})

MDA-MB-231 (MM231)

PP1 analogue kinase inhibitor 1-(1,1-dimethylethyl)-3-(1-naphthalenylmethyl)-1H-pyrazolo[3,4-d] pyrimidin-4-amine (NM-PP1)

focal adhesion (FA)

doxycycline (DOX)

inducible knock-down (iKD)

reverse-phase protein array (RPPA)

Basement Membrane Extract (BME)

tyrosine 234 (Y234)

co-immunoprecipitation (coIP)

Plasminogen Activator Inhibitor 1 (*PAI1*)

Smad Anchor for Receptor Activation (SARA)

Isopropyl β-D-1-thiogalactopyranoside (IPTG)

N-benzyl (Bn)-ATPγS

Tris-Buffered Saline (TBS)

Enhanced Chemo-Luminescence (ECL)

Paraformaldehyde (PFA)

Introduction

Metastasis underlies the mortality in most high-grade and triple negative breast cancer (TNBC) patients (Kirsch and Loeffler, 2005). Clinical management of these aggressive breast cancer types is challenging due to a lack of responses to standard chemotherapy treatment and hormone receptor antagonist regimens (Aversa *et al.*, 2014; Kennecke *et al.*, 2010). Together, these features underscore an unmet need: the identification of markers that identify drug benefit and/or allow targeted intervention of high-risk breast cancers.

The FPS/FES-related non-receptor tyrosine kinase FER was identified as a promising candidate for targeted therapy of metastatic breast cancer (Ivanova *et al.*, 2013; Tavares *et al.*, 2022). Yet, caveats in using such approach rely on FER´s role in regulating normal inflammation and innate immunity (Craig and Greer, 2002) and the inexistence of specific FER inhibitors. FER kinase regulates cell-cell and cell-matrix contacts, possibly through interaction with adherens junction components p120-catenin and β-catenin (Greer, 2002), by controlling actin polymerization (Ladwein and Rottner, 2008) or through down-regulating the synthesis of glycans that bind to the basement membrane protein laminin (Yoneyama *et al.*, 2012). Moreover, FER controls cell cycle progression and promotes integrin-dependent cell migration and invasion (Arregui *et al.*, 2000; Ivanova *et al.*, 2013; Kapus *et al.*, 2000; Kim and Wong, 1995). High FER levels have been linked to ovarian, renal and colon cancer progression (Allard *et al.*, 2000; Kawakami *et al.*, 2013; Li *et al.*, 2009; Menges *et al.*, 2010; Takeshima *et al.*, 1998; Zirngibl *et al.*, 2001). In breast cancer, FER expression is an independent predictor of survival, especially in lymph-node negative patients (Ivanova *et al.*, 2013). Elevated FER levels correlate with high grade breast cancer types such as TNBC and breast cancer brain metastasis (Ivanova *et al.*, 2013; Oshi *et al.*, 2020). Moreover, FER promotes growth and dissemination of melanoma and breast cancer cells in mouse models (Ivanova *et al.*, 2013, 2019). Apart from tyrosine phosphorylation of p120-catenin, β-catenin, the actin-binding protein Cortactin (Kim and Wong, 1998) and the microtubule interactor CRMP2 (Zheng *et al.*, 2018), functional data on direct FER substrates are currently scarce and limited to DCTN2 and MAPK1 (Tavares *et al.*, 2022).

Sno/Ski family members have been linked to transforming growth factor β (TGFβ) and bone morphogenic protein (BMP) signaling pathways, possibly through binding and antagonizing Smad proteins (Akiyoshi *et al.*, 1999; Luo, 2004; Luo *et al.*, 1999). Although Sno and Ski are classified as proto-oncogenes, their exact role in tumor progression remains largely unknown. All Sno/Ski family members feature a conserved Sp100/AIRE-1/NucP41/75/DEAF-1 (SAND) motif within their Ski homology domain (Wu *et al.*, 2002). The SAND domain is present in a subset of nuclear proteins that are involved in chromatin-dependent transcriptional regulation (Bottomley *et al.*, 2001). An interaction loop (I-loop) within the SAND domain allows these proteins to bind DNA (Bottomley *et al.*, 2001; Wu *et al.*, 2002). In addition, it has been described that Ski, SnoN and SKOR2 can interact with Smad2/3 through their N-terminal regions and with Smad4 through their SAND domains (Wu *et al.*, 2002).

SKOR1, or functional Smad suppressor element on chromosome 15 (Fussel-15), is the most recently identified member of the Sno/Ski family (Arndt *et al.*, 2007). Human SKOR1 is primarily, but not exclusively, expressed in the central nervous system in the migratory precursors of cerebellar Purkinje cells (Arndt *et al.*, 2007). SKOR1 can act as a transcriptional co-repressor with homeodomain transcription factor Lbx1, thereby regulating the cell fate of dorsal horn interneurons (Mizuhara *et al.*, 2005). Recent evidence implicates a role for SKOR1 in restless leg syndrome and transcriptional regulation of genes involved in neurodevelopment and iron metabolism (Sarayloo *et al.*, 2020). Additionally, activated fibroblasts express SKOR1 during early phases of wound healing, where it promotes fibroblast migration and affects F-actin and focal adhesion distribution (Arndt *et al.*, 2011). Moreover, the Drosophila homologue of SKOR1, Fuss, inhibits differentiation and sustains proliferation in developing eye imaginal discs (Rass *et al.*, 2022). In cancer, functions for SKOR1 have remained largely unexplored, except for a recent study observing SKOR1 expression in breast cancer metastasis to the brain (Oshi *et al.*, 2020).

Based on a chemical genetics approach, we have identified and validated SKOR1 as a direct substrate of the non-receptor tyrosine kinase FER. Our data demonstrate that SKOR1 is essential for tumor growth and invasion, functions that are dependent on the candidate FER phosphorylation tyrosine residue Y234 in SKOR1.

Results

FER kinase activity controls invasion and metastasis formation in TNBC

Previous studies have established FER as a driver of invasion and metastasis formation in high grade and basal-like breast cancers (Ivanova *et al.*, 2013). To study if FER relies on its kinase activity to drive tumor progression, we generated a FER analogue-sensitive (FER-AS) knock-in allele (FER^{ASKI}) in MDA-MB-231 (MM231) cells using CRISPR-Cas9 gene editing (Fig. S1A-D). To do so, the gatekeeper residue in the kinase active site of endogenous FER was mutated, which results in an enlarged ATP-binding pocket. Mutation of methionine 637 to alanine in FER confers unique sensitivity to chemically modified derivatives of PP1, the Src-family-selective inhibitor (Bishop *et al.*, 1999, 2000). Knock-in of the gatekeeper mutation (M637A) results in near-endogenous expression levels of FER-AS when compared to MM231 parental cells (Fig. S1E). Importantly, analogue-sensitive kinase inhibition using the PP1 analogue kinase inhibitor 1-(1,1-dimethylethyl)-3-(1-naphthalenylmethyl)-1H-pyrazolo[3,4-d] pyrimidin-4-amine (NM-PP1) does not influence expression of FER-AS (Fig. S1E) but leads to decreased tyrosine phosphorylated on several proteins (Fig. S1F). Whereas no effect is observed in control MM231 cells (Fig. S1G to J and (Tavares *et al.*, 2022)), treatment of FER^{ASKI} cells with 1 µM NM-PP1 leads to a spread and sessile phenotype accompanied by abundant stress fibers and focal adhesion (FA) formation (Fig. 1A and

1B), indicating that this phenotype is a result of specific inhibition of FER kinase activity. Adding to this, we observed no significant changes in activation of other tyrosine kinases, such as Src, upon treatment of NM-PP1 on parental MM231 cells (Fig. S1K). As loss of FER was shown to inhibit cell cycle progression and impair proliferation of MM231 cells (Ivanova *et al.*, 2013; Pasder *et al.*, 2006), we further explored the role of its kinase activity in regulating TNBC cell proliferation. FER kinase inhibition in FER^{ASKI} interphase cells using NM-PP1 results in a modest but not significant decrease in proliferation (Fig. S1J). As control, we treated MM231 FER iKD (cultured in the presence or absence of DOX) with or without NM-PP1 and neither observed differences in FER protein levels, nor a significant reduction in proliferation (Fig. S1L-M and I). Importantly, however, addition of NM-PP1 impairs cell motility in 2D (Fig. 1C). While proliferation is not significantly affected upon specific FER kinase inhibition in 3D cultured cells (Fig. 1D and quantified in Fig. S1N), invasion is significantly impaired upon treatment with NM-PP1 (Fig. 1D-E). Combined, these results provide formal evidence that FER regulates tumor cell invasion and migration through its tyrosine kinase activity.

Although FER depletion is sufficient to inhibit metastasis formation of MM231 cells in mice (Ivanova *et al.*, 2013), it remained unclear if this was due to inhibition of its tyrosine kinase activity. To test this, we orthotopically transplanted luciferase-tagged FER^{ASKI} cells in recipient immune-deficient mice and started treatment with NM-PP1 upon formation of palpable primary tumors (~ 50 mm^3). Tumor growth was monitored longitudinally, and mice were sacrificed once lung metastases were detected by bioluminescence imaging. We do not observe differences in primary tumor volumes between the treated and untreated cohorts (Fig. 1F and quantified in Fig. S1O), in agreement with published findings showing that loss of FER function *in vivo* mainly affects invasion and metastasis (Ivanova *et al.*, 2013). Untreated animals show a median metastasis-free latency of approximately 22 days (Fig. 1G), supporting published findings using FER loss (Ivanova *et al.*, 2013) and showing that the FER^{ASKI} allele is fully functional *in vivo*. In contrast, inhibition of FER kinase activity with NM-PP1 delays the median development of metastasis to 28 days when compared to the control group (p=0.006; Fig. 1G). NM-PP1-treated mice develop tumors that show reduced local invasion in the surrounding tissue compared to control mice (Fig. 1H). Together, these results demonstrate that FER kinase activity promotes tumor invasion and metastasis of TNBC cells in mice.

To analyze the impact of FER on phosphorylated downstream effectors, we used a Doxycycline (DOX)-inducible FER knock-down (FER iKD) combined with a reverse-phase protein array (RPPA) analysis (Fig. S2A and SFig.3A). Expression and phosphorylation were assayed using stable FER iKD in two high grade basal breast cancer cell types, MM231 (Fig. S2B and Table S1) and SUM149PT (Fig. S3B and Table S2). The changes observed in a range of signaling proteins and phosphoproteins upon the inducible FER knockdown in MM231 and SUM149PT cells demonstrate that FER drives crucial signaling pathways in both cell types. DOX-induced loss of FER expression attenuates the activation of multiple key signaling pathways in MM231 cells (Table S1), such as Rb phosphorylation at Ser807 and Ser780 (Fig. S2C), sites

required for G0-G1 transition (Ren and Rollins, 2004). In line with the kinase-specific inhibition of FER (Fig. S1F), we found that EGFR Tyr1173 phosphorylation is reduced upon loss of FER in MM231 cells (Table S1), confirming EGFR as a FER downstream target (Guo and Stark, 2011; Tavares *et al.*, 2022). Moreover, we observed altered levels of VEGFR-Tyr1175, PDGFR-Tyr1021 and IGF1R-Tyr1162/3 phosphorylation upon FER loss (Table S1 and Table S2), suggesting that FER indirectly controls the function and/or processing of multiple growth factor receptors. Interestingly, Smad2/3 phosphorylation levels are consistently decreased after FER loss on several Serine epitopes in both cell systems used (Table S1 and Table S2), which suggests a role for the regulation of TGFβ/BMP signals by FER.

SKOR1 is a direct FER substrate that promotes migration and invasion

We have recently performed chemical genetics (Bishop *et al.*, 2000) using a truncated version of FER-AS to identify direct FER kinase substrates (Tavares *et al.*, 2022). From these targets we selected SKOR1, a Sno/Ski family member that is classified as a proto-oncogene. SKOR1 was selected because it has been linked to the regulation of BMP signaling through interaction with Smads (Arndt *et al.*, 2007; Gray *et al.*, 2019), its expression has been observed in breast cancer brain metastases (Oshi *et al.*, 2020), and its role in tumor progression remains largely unknown. We validated SKOR1 as a direct FER substrate *in vitro* using a GST fusion protein containing SKOR1 exon 5 and ATP incorporation (Fig. 2A-B). SKOR1 phosphorylation is specific, because either using a kinase-dead FER (D742R) or pharmacological inhibition of the gatekeeper FER kinase using NM-PP1 significantly inhibits SKOR1 phosphorylation (Fig. 2A-B). Moreover, phosphorylation is reduced when using SKOR1-Y^{NULL}, a SKOR1 mutant in which all tyrosine residues in exon 5 are mutated to alanine (Fig. S4A), indicating that FER-dependent phosphorylation occurs specifically on tyrosine residues.

To analyze the role of SKOR1 in high grade metastatic breast cancer cells, we performed a stable knock-down of SKOR1 in MM231 using two independent shRNA hairpins (Fig. 2C-E). SKOR1 mRNA levels were stably and consistently reduced to approximately 50% in multiple independent experiments (Fig. 2C). Reducing SKOR1 levels using either hairpin results in a stark reduction in cell numbers compared to the scrambled control shRNA (compare day 1 to day 4, Fig. S4B), suggesting that SKOR1 is necessary for cell proliferation and survival. After stable integration and selection, we could confirm that SKOR1-depleted cells display a decreased proliferative capacity (Fig. 2E). Strikingly, loss of SKOR1 phenocopies FER depletion (Ivanova *et al.*, 2013) and inhibition (Fig. 1A and Fig. 2D), including extensive cell spreading and collective growth as non-motile cells. SKOR1 depletion also induces loss of lamellipodia and F-actin stress fiber formation in 2D (Fig. 2D), a characteristic feature of FER loss or inhibition in MM231 cells (Ivanova *et al.*, 2013) and Fig. 1A).

To temporally and reversibly control the SKOR1 knock-down, we employed a DOX-inducible lentiviral shRNA system in MM231 and SUM149PT cells, which reproducibly resulted in a 50% reduction of SKOR1 expression after induction (SKOR1 iKD; Fig. 2F and Fig. S5A). Inducible SKOR1 loss causes extensive cell

spreading, formation of stress fibers (Fig. 2G and Fig. S5B) and a significant increase in FA formation (Fig. 2H and Fig. S5C). In addition, we observed that SKOR1 knock-down leads to impaired 2D proliferation of MM231 cells (Fig. 2I) and impairment of single cell migration when compared to cells cultured in control conditions in both MM231 and SUM149PT cell lines (Fig. 2J and Fig. S5D).

We next cultured MM231 SKOR1 iKD cells in 3D basement membrane extract (BME) gels and observed that SKOR1 depletion fully prevents invasion when compared to control spheroids that exhibit highly branched, invasive and disorganized colonies (Fig. 2K and 2M). Because SKOR1-depleted cells show clear growth defects when cultured in 2D, we assessed proliferation and apoptosis using BrdU incorporation and cleaved caspase-3 as markers, respectively. These analyses indicate that the reduction in colony formation upon SKOR1 depletion is mainly due to an impairment in proliferation in 3D (Fig. 2L) because we observed no differences in apoptosis compared to controls (Fig. 2K).

SKOR1 tyrosine 234 is required for cellular proliferation and invasion

Our chemical genetics and proteomics studies had identified SKOR1-Tyrosine 234 (Y234) as a candidate FER phosphorylation site, a residue that resides in the I-loop of the SAND domain (Fig. 3A) (Arndt *et al.*, 2007). We therefore stably expressed a GFP-tagged and RNAi-resistant wild-type (WT) SKOR1 cDNA, or a SKOR1 cDNA harboring a phenylalanine at position 234 (Y234F) in MM231 SKOR1 iKD cells ($SKOR1^{RECON}$; Fig. 3B), which prevents phosphorylation of SKOR1-Y234 without altering the protein structure. Upon SKOR1 reconstitution, we observed that the WT cDNA fully rescues the SKOR1 knock-down phenotype, presenting a migratory and spindle-like morphology resembling the parental MM231 morphology (Fig. 3C, upper panels). Conversely, $SKOR1^{RECON}$::Y234F cells fail to migrate and exhibit a spread and sessile phenotype (Fig. 3C, bottom panels). Impairment of migration in $SKOR1^{RECON}$::Y234F cells coincides with the formation of stress fibers and a marked increase in the number of FA sites (Fig. 3C, quantified in Fig. 3D), which suggests that the SKOR1 Y234 residue is involved in the regulation of F-actin dynamics and FA formation in MM231 cells. In line with these observations, overexpressing $SKOR1^{WT}$ in control cells does not affect migration or FA dynamics, whereas overexpressing $SKOR1^{Y234F}$ in control cells reduces migration and disturbs FA dynamics compared to control or $SKOR1^{WT}$ overexpressing cells (Fig. S6B-D). These results suggest that high expression of $SKOR1^{Y234F}$ is sufficient to overtake/interfere with the role of endogenous SKOR1 in regulating cell migration and FA organization.

$SKOR1^{WT}$ and $SKOR1^{Y234F}$ localize throughout the cytosol in vesicular-like structures that are most prominent in the perinuclear region (Fig. 3C and Fig. S6B). Interestingly, reconstitution with $SKOR1^{Y234F}$ results in a 60% decrease in cellular proliferation in 2D compared to $SKOR1^{WT}$ (Fig. 3E). Next, we assessed 3D cancer cell invasion, proliferation and apoptosis. We unexpectedly observe that the SKOR1-Y234 residue does not significantly contribute to cellular proliferation, nor apoptosis in this setting (Fig. 3F and 3G). However, the $SKOR1^{Y234F}$ mutant is unable to rescue invasion of MM231 cells in 3D (Fig. 3F,

quantified in Fig. 3H). Together, our results show that SKOR1-Y234, a FER kinase candidate substrate residue, is necessary for the invasion of the triple negative MM231 cells.

Because of the overlap in phenotype upon inhibition of FER kinase activity with NM-PP1 or depleting SKOR1, we used the FER^{ASKI} model and transduced SKOR1^{WT} or SKOR1^{Y234F} to assess functional interdependence. Control FER^{ASKI}::SKOR1^{WT} cells display a highly invasive phenotype, with lamellipodia formation and spindle-like shaped cells (Fig. 4A). SKOR1^{WT} fully prevents the phenotypical consequences of FER kinase inactivation in the presence of NM-PP1, sustaining a spindle-like and motile cell phenotype with sparse FA sites (Fig. 4A, bottom panels and Fig. 4B). Control FER^{ASKI}::SKOR1^{Y234F} cells exhibit a mixed/hypomorphic phenotype, whereby migratory cells coincide with cells that show extensive cell spreading and an increase in FA formation (Fig. 4A and 4B). Inhibition of FER kinase activity using NM-PP1 induces a further increase in cell spreading and an accompanying transition from a spindle-like cell shape to a spread phenotype with an increased number of FA sites in FER^{ASKI}::SKOR1^{Y234F} cells (Fig. 4A and 4B). Overexpression of SKOR1^{WT} in NM-PP1 treated FER^{ASKI} cells results in a minor but not significant increase in cell proliferation in 2D (Fig. 4C)), suggesting a compensatory effect of SKOR1^{WT} overexpression when FER kinase activity is reduced. Interestingly, proliferation defects are observed in FER^{ASKI}::SKOR1^{Y234F} cells treated with NM-PP1 (Fig. 4C), indicating that SKOR1-Y234 is involved in TNBC cell proliferation.

We also studied the effect of the SKOR1-Y234 residue on 3D invasion in the context of FER kinase function and observed that SKOR1^{Y234F}, in contrast to SKOR1^{WT}, is unable to rescue the impaired invasive growth caused by FER inactivation (Fig. 4D). Treatment with NM-PP1 leads to a full inhibition of both invasion and proliferation in FER^{ASKI}::SKOR1^{Y234F} cells, whereas FER^{ASKI}::SKOR1^{WT} cells form highly invasive structures upon NM-PP1 treatment (Fig. 4D-F). These data suggest that the SKOR1^{Y234} residue functions downstream of FER kinase to promote tumor cell proliferation and invasion of high-grade breast cancer cells.

SKOR1 regulates BMP/TGFβ signaling and binds Smad2/3 in TNBC cells.

We next tested if SKOR1-Y234 modulation leads to phosphorylation changes in signaling pathways. For this we used RPPA combined with SKOR1 reconstitution in MM231 SKOR1 iKD cells (Fig. 5A and Table S3). Reconstitution with SKOR1^{Y234F} reduces phosphorylation of EGFR signaling and its downstream effectors such as 4EBP1 and MAP kinase on multiple epitopes (Fig. 5B, right panel, and Table S3). When comparing SKOR1^{Y234F} cells to FER iKD cells, we observed that many substrates altered by SKOR1^{Y234F} expression are similarly affected by FER depletion, including Rb (Ser780, Ser807), mTOR and EGFR (Tyr1173) (Fig. 5B). Importantly, like in FER-depleted cells, SKOR1^{Y234F} reconstitution leads to a decrease in Smad2/3 phosphorylation (Ser423, Ser425, Ser467/Ser425) (Fig. 5B), which is in concordance with reported links of SKOR1 to BMP/TGFβ signaling (Arndt *et al.*, 2007; Fischer *et al.*, 2012; Takaesu *et al.*, 2012). To verify possible ties between SKOR1 and Smad signaling, we assessed SKOR1 binding to Smad.

For this, we performed co-immunoprecipitation (coIP) assays in SKOR1^{RECON} cells, which confirmed that SKOR1^{WT} precipitates with Smad2 and Smad3, whereby we noted a higher affinity to Smad3 (Fig. 5C). SKOR1^{Y234F} reconstitution increases binding to Smad3 compared to SKOR1^{WT} (Fig. 5C, quantified in Fig. 5D), suggesting that phosphorylation of Y234 in SKOR1 weakens binding to Smad3. Because Smad3-dependent transcription activation downstream of TGFβ/SMAD signaling pathway depends on Smad3 translocation to the nucleus, we applied the $CAGA_{12}$-luciferase transcriptional reporter as an indirect readout of nuclear Smad3 activation (Dennler *et al.*, 1998). Either FER depletion or SKOR1 reconstitution with the Y234F mutant (Fig. 5E) leads to a significant decrease of Smad3-dependent transcriptional activity. To further assess if FER and SKOR1 impact Smad3-dependent signaling pathways, we assessed the mRNA levels of plasminogen activator inhibitor 1 (PAI1), a Smad3 effector that is specifically upregulated in Smad3-driven tumor progression (Petersen *et al.*, 2010). Either FER or SKOR1 loss leads to a decrease in PAI1 mRNA expression in MM231 cells (Fig. 5F). We also observe that PAI1 expression is significantly decreased upon SKOR1^{Y234F} reconstitution (Fig. 5F). Together, these data suggest that FER-dependent phosphorylation of SKOR1 on Y234 may regulate binding of SKOR1 to Smad3, thereby facilitating phosphorylation and activation of Smad3-dependent signals.

SKOR1 promotes tumor growth and metastasis in mouse xenografts.

We next orthotopically transplanted luciferase-expressing MM231 SKOR1 iKD cells in recipient female mice and measured primary tumor growth and metastasis development over time. As SKOR1 loss inhibits proliferation in MM231 cells, we transplanted untreated cells, monitored animals until palpable tumors (~50 mm3) formed in both groups and started DOX administration to induce SKOR1 knock-down. Real-time qPCR was used to quantify SKOR1 mRNA in tumor samples, which confirms our *in vitro* data that SKOR1 expression is downregulated to approximately 50% after knock-down when compared with controls (Fig. 6A). In contrast to FER kinase inhibition, SKOR1 loss significantly affects primary tumor growth (Fig. 6B). Moreover, bioluminescence imaging showed that SKOR1 loss impairs the development of lung metastases, leading to an increased metastasis-free survival (Fig. 6C and 6D). In contrast to control tumors, SKOR1-depleted tumors tend to show expansive growth patterns with little to no invasion into the stroma and adjacent muscle layers of the mammary fat pad (Fig. 6E). From these results we conclude that SKOR1 promotes tumor growth and metastasis of high grade and basal-like breast cancer cells in mice, suggesting that SKOR1 contributes to tumor progression in breast cancer.

Discussion

Because SKOR1 expression has been predominantly observed in brain tissues, most studies have focused on its role during neuronal development (Arndt *et al.*, 2007). Now, our study identifies SKOR1 as a direct FER substrate *in vitro* and an important regulator of breast cancer growth and metastasis formation *in vivo*. We propose that SKOR1 plays a key role in promoting cell proliferation and migration,

thereby driving tumor progression and metastasis formation. Interestingly, SKOR1 expression has been associated with migration of other cell types. SKOR1 is expressed in Purkinje cells throughout all stages of embryonic development and in adulthood, with particularly high levels noted in the migratory precursors of Purkinje cells (Arndt *et al.*, 2007). In early stages of wound healing, SKOR1 expression is upregulated in fibroblasts, where it may control cellular migration by affecting F-actin dynamics and/or organization (Arndt *et al.*, 2011). Elevated SKOR1 levels are sustained in the fibro-proliferative diseases keloid scars and skin sclerosis (Arndt *et al.*, 2011), possibly contributing to the pathogenesis of these diseases by promoting the migration of dermal fibroblasts into the wound site, reorganizing the collagen structure that is deposited by these fibroblasts, and controlling collagen contraction (Arndt *et al.*, 2011). In line with our data showing that SKOR1 loss induces stress fiber and FA formation and impairs migration, overexpression of SKOR1 in fibroblasts promotes cell motility by driving F-actin and FA complex redistribution at the cell periphery (Arndt *et al.*, 2011). Based on these observations and our findings, SKOR1 appears to play a critical role in regulating cytoskeletal organization to control cell morphology and promote cell motility (Arndt *et al.*, 2011).

Here, we propose that SKOR1 acts downstream of FER, because SKOR1 loss of function phenotypes are virtually identical to FER kinase inactivation (Ivanova *et al.*, 2013; Sangrar *et al.*, 2007). Although the kinase activity of FER appears to only modestly contribute to the proliferation of MM231 cells, SKOR1 loss of function profoundly impacts cellular growth. While we have no clear hypothesis or data explaining the mechanism that controls inhibition of proliferation upon SKOR1 knock-down, we also cannot exclude the possibility that phosphorylation of SKOR on Y234 by FER induces pro-proliferative cues stemming from SKOR1.

In previous studies we determined that FER regulates actin dynamics and FA distribution via endosomal recycling of growth factor receptors and cell adhesion molecules, and that dysregulation of membrane trafficking upon FER depletion greatly impairs the migratory and invasive behavior of breast cancer cells (Ivanova *et al.*, 2013; Tavares *et al.*, 2022). Because SKOR1 belongs to a well-known family of major regulators of TGFβ signaling, a pathway for which endosomal recycling of TGFβ receptors is essential (Yakymovych *et al.*, 2017), we decided to examine if SKOR1 promotes FER-dependent cytoskeletal organization and invasion in TNBC through TGFβ signaling. In early endosomes, signaling-promoting factors such as SARA (Smad Anchor for Receptor Activation) support Smad2/3 and TGFβ receptor interaction, which facilitate TGFβ signaling and downstream Smad2/3 phosphorylation (Chen, 2009; Nawshad *et al.*, 2005). Phosphorylated Smad2/3 forms a heterotrimeric complex with Smad4 that translocates to the nucleus where it associates with transcription factors and coregulators to control expression of >500 specific target genes (Tecalco-Cruz *et al.*, 2018). Interestingly, our results show that loss of FER expression and SKOR1^{Y234F} substitution similarly affect (phosphorylation) levels of several growth factor receptors and downstream signaling factors, including decreased phosphorylation of TGFβ signaling mediators Smad2/3. Like SARA, Ski, SnoN, and SKOR2 are Smad-interacting proteins

that regulate TGFβ signaling through simultaneous interaction with Smads (Tecalco-Cruz *et al.*, 2018; Wu *et al.*, 2002). Interestingly, we find that SKOR1 preferentially binds to Smad3 in TNBC cells, an observation that agrees with previous reports (Arndt *et al.*, 2007; Takaesu *et al.*, 2012). While Ski and SnoN proteins mainly localize to the nucleus to bind Smad4 and act as transcriptional corepressors through the I-loop of their SAND-domain (Nicol *et al.*, 1999; Nicol and Stavnezer, 1998), SKOR1 shows a predominant cytoplasmic and vesicular-like localization in MM231 cells, suggesting control over Smad3 in the cytosol. Our data indicate that FER phosphorylates SKOR1 on tyrosine Y234, a residue located in the I-loop of SKOR1 (Arndt *et al.*, 2007), and that loss of function phenylalanine exchange at this site increases Smad3 binding to SKOR1. These results suggest that FER-dependent SKOR1 phosphorylation promotes dissociation of SKOR1-Smad2/3 complexes and thereby potentiates TGFβ signaling through a release of Smad2/3 molecules and subsequent recruitment by signaling-promoting factors such as SARA (Fig. 6F). Furthermore, we suggest that potentiation of TGFβ signaling through releasing Smad3 upon phosphorylation of SKOR1-Y234 by FER leads to transcriptional expression of *PAI1*, a known player in cancer progression (Petersen *et al.*, 2010). *PAI1* expression is known to induce tumor angiogenesis (Isogai *et al.*, 2001) and promotes breast cancer cell migration through induction of F-actin-dependent formation of membrane protrusions (Chazaud *et al.*, 2002; Liu *et al.*, 2020). Hence, although the exact mechanism whereby SKOR1 regulates FA distribution and actin dynamics is still unclear, these studies suggest that SKOR1 activity can induce cytoskeletal organization and promote cell migration possibly through Smad3 signaling and *PAI1* expression. It has also been reported that Smad3 can upregulate the expression of ubiquitin ligases that target RhoA for degradation (Yu *et al.*, 2015). Activation of RhoA is essential for FA assembly and stress fiber formation (Aguilar-Rojas *et al.*, 2012).. Because we observed these features in SKOR1-depleted and SKOR1^{Y234F} expressing cells, it suggests that SKOR1 loss or SKOR1^{Y234F} expression might cause sustained RhoA activity by decreasing Smad3 signaling, thereby inducing F-actin bundling and FA formation. Conversely, SKOR1-Y234 phosphorylation by FER could promote Smad3-dependent degradation of RhoA, leading to F-actin redistribution and disassembly of FAs to increase cell migration and invasion.

In closing, we present evidence that SKOR1 mediates FER-dependent tumor cell migration and invasion in breast cancer cells through regulation of actin cytoskeleton dynamics and FAs formation. Our data show that the SKOR1 tyrosine 234 residue, a candidate FER kinase phosphorylation site, is critical for the invasive growth of basal-type breast cancer cells. Although further studies will be needed to provide formal proof for phosphorylation of SKOR1-Y234 *in vivo*, our work substantiates FER as a cardinal tumor progression factor and advocates inhibition of FER kinase activity as a promising intervention for high-grade and basal-type breast cancers.

Materials & Methods

Constructs, virus generation and transduction

SKOR1 Exon 5 wild type (WT) and Y^{NULL}, in which all tyrosine residues were substituted by alanine residues, were ordered as gene blocks, subcloned in the pJET1.2/blunt cloning vector (Fermentas by Thermo Scientific, St. Leon-Rot, Germany) and inserted into the *Not*I/*Eco*RI sites of pGEX-6P-1 to introduce the GST tag. For stable knock-down (KD) of SKOR1, human SKOR1 shRNA pLKO.1-puro constructs were used (#1: 5′-CGAGCCAGATAAGGAAGACAA-3′, #2: 5′-CCTATCCAGACCAAAGGAGTA-3′). pLKO.1-TRC (shSCR) (Addgene; 10879) was used as a control. The inducible SKOR1 RNAi system was generated as described previously using the shSKOR1 #1 sequence (Schackmann *et al.*, 2011). To generate GFP-SKOR1-expressing constructs, full length SKOR1 cDNA was obtained from transOMIC (BioCat, gene ID 390598) and was cloned into a Gateway-compatible entry vector (Thermo Fischer scientific) (pENTR-SKOR1), and subsequently recombined into destination vectors using the Gateway™ LR Clonase™ II Enzyme Mix (Invitrogen, 11791-020, Carlsbad, CA, USA). Mutations were introduced in pENTR-SKOR1 following the QuikChange II XL Site-Directed Mutagenesis protocol (QuikChange; Agilent Technologies, Wilmington DE). Three silent mutations were introduced to create resistance to sh901 (SKOR1-shRes) using primers 5′-GAAACGAGGAAATCCTA**C**CCAGACCAAAG**A**AG**C**ATCTCCCAGCC-3′ (forward) and 5′-GGCTGGGAGAT**G**CT**T**CTTTGGTCTGG**G**TAGGATTTCCTCGTTTC-3′ (reverse). The Y234F mutation was introduced using primers 5′-CCGACGCCAAGTTCACGCAGCCCGA-3′ (forward) and 5′-TCGGGCTGCGTGAACTTGGCGTCGG-3′ (reverse), generating pENTR-SKOR1-shRes-Y234F. SKOR1-shRes-WT and -Y234F were then recombined into pLenti CMV-GFP (658-5) (Addgene; 17448). For transduction of the above-mentioned constructs, pLV-PGK-GFP (Addgene; 19070) was included as a control. Lentivirus was produced in HEK239T cells, followed by cell transduction as described previously (Schackmann *et al.*, 2011) and one week of puromycin selection (2 μg/ml) for stable SKOR1 KD MM231 cells. For CRISPR-based gene editing, oligo's encoding single guide RNA sequences targeting FER (sense: 5′-AAATCCTTGGAGACTTTACG-3′ and anti-sense: 5′-CGTAAAGTCTCCAAGGATTT-3′) were annealed by heating to 95°C, followed by a gradual cool-down to room temperature. Annealed oligos were ligated into *Bbs*I-digested pACEBac1-Cas9-GFP. Left and right homology arms (LHA and RHA, respectively) were designed according to the In-Fusion cloning strategy and ordered as gene blocks (Supplementary info). Each homology arm was subcloned into the pJET1.2/blunt cloning vector (Fermentas by Thermo Scientific, St. Leon-Rot, Germany) and inserted into pUNKI-puro (kindly provided by S. Lens, University Medical Center Utrecht). LHA was first ligated into the *Cla*I/*Asc*I sites of pUNKI, followed by ligation of RHA into the *Sac*I/*Sal*I sites to generate pUNKI-puro-LHA-RHA. The puro-LHA-RHA cassette was then inserted into the gRNA-containing pACEBac1-Cas9-GFP by *Not*I restriction cloning, generating pACEBac1_FER-AS. All constructs were verified by Sanger DNA sequencing. Plasmids generated in this study can be obtained upon request.

Cell culture and transfection

MDA-MB-231 (MM231) cells were obtained from Cell Lines Service (Eppelheim, Germany) and SUM149PT were obtained from Asterand, Inc. (Detroit, MI, USA). Both were STR verified, and grown in DMEM growth medium (Invitrogen, 11039-047, Carlsbad, CA, USA), supplemented with 1% penicillin-streptomycin (Invitrogen, 15070-063, Carlsbad, CA, USA) and 10% fetal bovine serum (FBS) (Invitrogen 16050-122, Carlsbad, CA, USA). Cells were cultured at 37°C with 5% CO_2. MM231 FER iKD cells have been generated previously (Ivanova *et al.*, 2013). MM231 cells were transfected with pACEBac1_FER-AS using FuGene HD according to manufacturer's instructions. Two days after transfection, cells were treated with 2 µg/mL puromycin for one week, followed by single-cell expansion. Positive FER^{ASKI} clones were selected by PCR and sequencing with primers 5'-TGAGGGAAGGCTTTACTCGTT-3' (forward) and 5'-TCCTTGGAGACTTTACGAGGAG-3' (reverse). MM231 FER^{ASKI} cells and MM231 parental cells were treated with 1 µM NM-PP1 (Calbiochem) for 3 days. DOX-inducible cell lines were treated for five days with 2 µg/mL Doxycycline (Sigma-Aldrich, D9891-1G), refreshed on day 3.

For 3D assays, MM231 cells were added to Cultrex Basement Membrane Extract (BME) (Trevigen; 3533-005-02) at a density of 500 cells/100 µL BME. Droplets of 25 µL were added to flat bottom, optical plastic 24-well plates (Corning, Tewksbury, USA). Plates were incubated for 45 min at 37°C to allow the BME to solidify, after which 500 µL normal growth medium was added. Cells were cultured for 7 days at 37°C. Cell lines generated in this study can be obtained upon request.

3D Morphology assessment

Brightfield images were acquired by using a 10× objective on an EVOS M5000 Imaging System (Thermofisher). At least 5 images were acquired per chamber well, and at least two wells were imaged per condition. Each image was segmented by individually optimizing the OrganoSeg (Borten *et al.*, 2018) parameters manually until a suitable segmentation was achieved. Invasiveness was inferred using 'Solidity' parameter (*Invasiveness=1-Solidity*) reported in each spheroid caption.

Expression of recombinant proteins and in vitro kinase assays

Protein expression in the *E. coli* strain Rosetta was induced by incubation with 0.2 mM isopropyl β-D-1-thiogalactopyranoside (IPTG) for 16h at 18°C. Recombinant proteins were extracted from bacterial pellets by adding lysis buffer (10 mM EGTA, 10 mM EDTA, 0,1% Tween 20, 250 mM NaCl, 5 mM DTT) supplemented with 0.325 mg/mL lysozyme and a cocktail of protease inhibitors (Roche, Complete™ EDTA free, Basel Switzerland). Samples were sonicated, centrifuged, and coupled to glutathione-Sepharose 4B beads (Amersham Biosciences), followed by elution with elution buffer (100mM Tris pH8.0, 30 mM GSH and 75 mM KCl). Eluates were treated with sample buffer (375 mM Tris-HCl pH 6.8; 25% glycerol; 12.5% β-mercapto ethanol 10% SDS: 0.025% bromophenol blue) and boiled. Proteins were separated on 15% SDS-PAGE gel and stained with Instant Blue.

Recombinant analogue-sensitive (AS) or kinase-dead (D742R) GST-FER were incubated with WT or Y^{null} exon 5 GST-SKOR1, or GST-Cortactin as substrate. Each reaction was performed in 25 µL kinase buffer (10 mM $MnCl_2$, 20 mM Tris-HCl pH 7.5, 0.1 mM sodium orthovanadate) supplemented with 250 µM N-benzyl (Bn)-ATPγS (B 072-05, BioLog), with or without 10 µM NM-PP1. After 30 min incubation at 30°C, reactions were terminated by addition of 2.5 mM EDTA were subsequently incubated with 2.5 mM p-Nitrobenzyl mesylate (Epitomics, Burlingame, CA) for 2h at room temperature. Reactions were stopped by adding sample buffer. The bio-orthogonal tiophosphate ester generated by the p-Nitrobenzyl mesylate was recognized by a thiophosphate ester-specific antibody.

Immunoblotting

Proteins were extracted from cells by scraping in sample buffer and lysed for 10 min on ice, followed by 10 min of boiling. Protein extracts and *in vitro* kinase reaction products were separated by SDS-PAGE electrophoresis and blotted onto PDVF membrane. Following 1 h blocking with 5% bovine serum albumin (BSA) in tris-buffered saline (TBS) 0.1% Tween-20, the membrane was incubated with primary antibodies in blocking buffer overnight at 4°C. After washing three times with PBS-Tween 0.1%, membranes were probed with either horseradish peroxidase-conjugated secondary antibodies (DAKO; 1:10,000) or IRDye 680- and 800-conjugated secondary antibodies (LI-COR; 1:5,000) for 1 h at room temperature and visualized using Enhanced Chemo-Luminescence (ECL)(GE Healthcare) or Typhoon Biomolecular Imager (GE Healthcare), respectively. The following primary antibodies and dilutions were used for western blotting: rabbit anti-phospho-Src (Invitrogen; 44-660G; 1:1,000), rabbit anti GAPDH (Sigma; G9545; 1:1,000), mouse anti-GAPDH (Millipore; Mab374; 1:1,000), rabbit anti-Thiophosphate ester (Abcam; ab92570; 1:5,000, UK), mouse anti-GST (Santa Cruz; sc-138; 1:1,000), mouse anti-GFP (Santa Cruz; sc-8334; 1:500), rat anti-GFP (3HG) (Chromotek; 029762; 1:1,000), goat anti-Akt (Santa Cruz; sc-1618; 1:1,000), mouse anti-pY20 (BD Biosciences; 610011; 1:1,000), rabbit anti-LBXCOR1 (Sigma; SAB2105374; 1:500), mouse anti-Smad2/3 (C-8) (Santa Cruz; sc-133098; 1:1,000), rabbit anti-phospho-EGFR Tyr1173 (Cell Signaling Technology; 4407; 1:500). The images of uncropped western blots are shown in Fig. S7.

3D invasion assay, BrdU incorporation and immunofluorescence

Invasion and proliferation were assessed by incubating cells in BME (3D) with 10 µm BrdU for 2 h. Cells were fixed with 4% paraformaldehyde (PFA) 1% Glutaraldehyde (Sigma, G5882), followed by 1% $NaBH_4$ treatment for 30 min. Then cells were washed with PBS before 2M HCl treatment for 80 min, Fixed cultures (3D) were blocked for overnight in 5% goat serum 0.3% Triton in PBS and incubated with 10 µL/mL Alexa 647-conjugated anti-BrdU antibody (BD biosciences, 560209) or anti-cleaved Caspase 3 (Cell Signaling, 9661s, 1:250) in 1% BSA 0.3% Triton in PBS overnight. Structures were washed three

times and then probed with secondary antibodies (when applicable), Alexa 568-conjugated Phalloidin (ThermoFisher; A12380; 1:200) and DAPI in 1% BSA 0.3% Triton in PBS overnight.

For 2D assays, cells were grown on 12 mm coverslips and fixed for 30 min using 4% PFA. Fixed cells were permeabilized with 0.1% Triton X-100 in PBS for 3 min, blocked with 5% BSA for 30 min and incubated with primary antibodies in 1% BSA in PBS overnight at 4°C. Cells were washed three times and then probed with secondary antibodies and Alexa 568-conjugated Phalloidin (ThermoFisher; A12380; 1:200) in 1% BSA for 2 h. After three washes in PBS, cells were stained with 2 µg ml^{-1} DAPI (Sigma; D9542) in 1% BSA for 5 min. Again, cells were washed thrice with PBS before mounting using ProLong Diamond Antifade (Invitrogen, Carlsbad, CA, USA). Primary antibody used was rabbit anti-phospho-Paxillin (Life Technologies, 447226; 1:200). Secondary antibody used was goat anti-rabbit Alexa-647 (Molecular Probes by Invitrogen, Carlsbad, CA, USA).

An inverted Carl Zeiss LSM 700 Laser Scanning Microscope with a Plan-Apochromat 63x/1.40 Oil DIC M27 or with a LD Plan-Neofluar 40x/0.6 Korr M27 objective was used for imaging. Confocal images were analyzed using ImageJ Software.

Co-Immunoprecipitation

GFP-tagged proteins were immunoprecipitated using a GFP-Trap system (Chromotek, gta-10) as described (Ven *et al.*, 2015). After washing with lysis buffer, bound and non-bound proteins were eluted in sample buffer, boiled, and analyzed by western blot.

Cell migration assay

The migratory abilities of MM231 overexpressing $SKOR1^{WT}$ or $SKOR1^{Y234F}$, MM231 SKOR1 iKD, SUM149PT SKOR1 iKD and MM231 FER^{ASKI} cells were assessed using live-cell imaging. MM231 SKOR1 iKD and SUM149PT SKOR1 iKD cells were induced for 5 days with or without DOX. MM231 FER^{ASKI} cells were treated for 3 days with NM-PP1 or DMSO (control), before plating them on 24-well plastic-bottom plates (Corning, Tewksbury, USA). MM231 SKOR1 iKD and $SKOR1^{RECON}$ cells were incubated with 200 nM SiR-DNA (Spirochrome) for 7-8 hours before imaging. SUM149PT SKOR1 iKD and MM231 cells expressing $SKOR1^{WT}$ or $SKOR1^{Y234F}$ were incubated with 1 µg/mL Hoechst for 10 min. Cells were imaged every 10 min for 16 h using a Carl Zeiss Cell Observer widefield microscope with an EC Plan-Neofluar 5x/0.16 M27 objective. During imaging, cells were kept in complete DMEM medium (with or without DOX, or with DMSO or NM-PP1) under normal growth conditions (37°C, 5% CO_2). Cell migration was quantified using the Imaris for Tracking software (Bitplane, Oxford Instruments, UK) or TrackMate (Tinevez *et al.*, 2017) plugins

Quantitative real-time PCR

Total RNA from the samples was extracted using RNeasy Plus Mini Kit (Qiagen, 74104) following the manufacturer's guidelines. cDNA synthesis was performed according to iScript cDNA Synthesis Kit (Bio-Rad). qPCR reactions were performed using FastStart Universal SYBR Green Master mix (Roche, 4913957001, Basel Switzerland) and Bio-Rad CFX96 touch Real-Time PCR detection system (Bio-Rad). mRNA levels were normalized to their corresponding GAPDH expression levels. Knock-down efficiency was quantified using the Pfaffl method (Pfaffl, 2001). Used oligonucleotide primer pairs: SKOR1 forward 5'-CCACGAGCCAGATAAGGAAG-3', SKOR1 reverse 5'-CCATTTGTTCCAGGAGCAGT-3', PAI1 Forward 5'-TCTTTGGTGAAGGGTCTGCT-3', PAI1 Reverse 5'-CTGGGTTTCTCCTCCTGTTG-3', GAPDH forward 5'-TGCACCACCAACTGCTTAGC-3' and GAPDH reverse 5'-GGCATGGACTGTGGTCATGAG-3'.

Colony formation assays

MM231 SKOR1 iKD cells were cultured with or without DOX for 5 days, and FER^{ASKI} cells were treated with DMSO or NM-PP1 for 3 days before seeding them at a density of 7,500 cells into each well of a 24-well plate and culturing them for 3 days. Cells were fixed using 10% Glutaraldehyde in normal growth medium for 10 min, stained using 0.1% crystal violet (Sigma) for 30 min while agitating, washed with water and dried overnight. Acetic acid 10% (v/v) was used to elute incorporated crystal violet for 30 min while agitating, after which the solution was quantified with a spectrophotometer at 590 nm (Bio-Rad).

Reverse protein phase array (RPPA)

MM231 SKOR1 iKD cells were cultured with or without DOX for 5 days, and FER^{ASKI} cells were treated with DMSO or NM-PP1 for 3 days. Cell extracts were prepared in RIPA (50 mM Tris-HCl pH 7.4, 150 mM NaCl, 1 mM EDTA pH 8.0, 1 mM EGTA, 1% Triton X-100, 0.1% SDS, 10 mM Glycerolphosphate, protease inhibitor cocktail (Complete, Sigma) and phosphatase inhibitor (Roche, phosSTOP, Basel Switzerland). RPPA was performed as described (Teo *et al.*, 2018).

SMAD3/SMAD4-dependent CAGA$_{12}$-luciferase transcriptional reporter assays

MMM231 FER iKD were treated with or without DOX for 5 days. SKOR1^{RECON}::WT and SKOR1^{RECON}::Y234F cells were treated with DOX for 5 days. Then, 50 thousand cells were plated in 6-well plates and transiently transfected with 0.4 µg the TGFβ/SMAD3-inducible $(CAGA)_{12}$ luciferase transcriptional reporter construct (Dennler *et al.*, 1998) and 1.44 µg of the internal control pRL-TK vector, using Lipofectamine 2000 (Alfagene, 11668-019) according to manufacturer's instructions. Cells were serum starved for 8 h before stimulation with 7 ng/mL of human recombinant TGFβ1 (Invitrogen, PHG9204) and luciferase activities were quantified 24 h later using the Dual Luciferase Assay (Promega, PROME1960010). Briefly, 80 µL of lysed samples were added to 100 µL of luciferase assay reagent II (LARII) in a 96-well plate. Firefly luminescence was detected using synergy Mx. Then, 100 µL of 1X Stop

and Glo solution were added to detect renilla luminescence. Each sample was evaluated in triplicates. Values were normalized with the renilla luciferase activity expressed from pRL-TK. Luciferase values shown in the figures are representative of transfection experiments performed in at least three independent experiments.

Mouse studies

Recipient female $RAG2^{-/-};IL2R\gamma c^{-/-}$ immunodeficient mice (Envigo) were orthotopically transplanted (in the inguinal mammary gland) with luciferase-expressing MM231 cells (FERASKI or SKOR1 iKD), using a 50-µL Hamilton syringe (Hamilton, Bonadur, Switzerland). Mice were anesthetized using isoflurane (IsoFlo; Le Vet Pharma). Burprenorphine (0.1 $mg \bullet kg^{-1}$) was injected subcutaneously as analgesic treatment. After a recovery period of 2 weeks, mice were anesthetized with IsoFlo, injected i.p. with 225 $\mu g \bullet g^{-1}$ body weight n-luciferin (potassium salt; Biosynth AG) and imaged on a Biospace Φ bioluminescence imager (Biospace Lab). Tumor growth was measured using a digital pressure-sensitive caliper (Mitutoyo) on a weekly basis. Treatment started when tumors reached a volume of 50-100 mm^3. To study *in vivo* inactivation of FER, FER^{ASKI} mice were switched to water containing DMSO (solvent) or NM-PP1 (25 µM, Merck) *ad libitum*. Drinking water was refreshed twice a week. To deplete SKOR1 in cancer cells, SKOR1 iKD mice were switched from standard diet to DOX containing chow (200 $mg \bullet kg^{-1}$; A155D70201; Ssniff, Bio services) *ad libitum*. Mice were euthanized if mammary tumor reached a size of 1000mm^3, in case of severe discomfort or when bioluminescence imaging revealed metastases.

Studies approval

All animal experiments were performed in accordance with local, national and European guidelines under permit AVD115002015263 issued by The Netherlands Food and Consumer Product Safety Authority (NVWA) of the ministry of Agriculture, Nature and Food.

Statistical analysis

Statistical analyses were performed using IBM SPSS Statistics (SPSS Inc., Chicago, IL, USA). The Kaplan-Meijer method was used for cumulative survival analysis; a two-way mixed model analysis of variance was used to evaluate differences in tumor volume. RPPA data were analyzed using an unpaired t-test with multiple comparison testing using the Benjamini, Krieger, and Yekutieli two-stage step up method of correction in Graphpad Prism. Z-scores are calculated as (Sample value – mean of antibody intensity across all samples)/standard deviation. Unbiased clustering was performed in Cluster 3.0 using Euclidean distance and average linkage and heatmaps were made in Java Treeview. All other data were analyzed using one-way ANOVA or unpaired t-test methods in Prism (Graphpad software version 8.0). No statistical method was used to predetermine sample size. No samples were excluded from the analyses.

All experiments were performed and quantified from at least three independent experiments (unless specified otherwise), and representative data are shown.

Online supplemental material

Fig. S1 shows how FER^{ASKI} cells were generated and validated. Fig. S2 shows that FER regulates key signaling pathways in MM231 breast cancer cells. Fig. S3 shows that FER regulates key signaling pathways in SUM149PT breast cancer cells. Fig. S4 shows that SKOR1 is necessary for proliferation of MM231 breast cancer cells. Fig. S5 show that SKOR1 is necessary for migration of SUM149PT cells. Fig. S6 shows that overexpression of SKORWT or SKORY234F impacts of migration of control MM231 cells. Fig. S7 shows the original blots cropped and shown in the other figures. We have also included the other replicates for experiments depicted in Figures S1E and 5C. Table S1 lists RPPA significant substrates upon FER depletion in MM231 cells. Table S2 lists RPPA significant substrates upon FER depletion in SUM149PT cells. Table S3 lists RPPA significant substrates upon $SKOR1^{Y234F}$ reconstitution in MM231 cells.

Acknowledgements

We thank Peter ten Dijke for reagents and comments on the manuscript. This research was supported by KWF Kankerbestrijding (UU2014-7201), The Netherlands Organization for Scientific Research (NWO-TOP 02007), and the European Union's Horizon 2020 FET Proactive program under the grant agreement No. 731957 (MECHANO-CONTROL).

Competing interests

The authors declare no conflict of interest.

Author contributions

Conceptualization, S.T. and P.W.B.D.; methodology, S.T. and P.W.B.D.; investigation, E.B., S.T., L.S., E. B., C.O., and L. E.; formal analysis, S.T., L.S., M.R., E. B. and L.E.; resources, M. H. and P. t. D.; writing—original draft, L. S. and S.T.; writing—review and editing, V.G. B, S.T. and P.W.B.D; funding acquisition, P.W.B.D; supervision, S. T. and P.W.B.D.

Funding

This work was supported by KWF Kankerbestrijding (UU2014-7201), The Dutch Research Council TOP grant (NWO-TOP 02007) and the European Union's Horizon 2020 FET Proactive program under the grant agreement No. 731957 (MECHANO-CONTROL).

References

Aguilar-Rojas, A., Huerta-Reyes, M., Maya-Núñez, G., Arechavaleta-Velásco, F., Conn, P.M., Ulloa-Aguirre, A. and Valdés, J. (2012), "Gonadotropin-releasing hormone receptor activates GTPase RhoA and inhibits cell invasion in the breast cancer cell line MDA-MB-231", *BMC Cancer*, Vol. 12 No. 1, p. 550.

Akiyoshi, S., Inoue, H., Hanai, J., Kusanagi, K., Nemoto, N., Miyazono, K. and Kawabata, M. (1999), "c-Ski Acts as a Transcriptional Co-repressor in Transforming Growth Factor-β Signaling through Interaction with Smads*", *Journal of Biological Chemistry*, Vol. 274 No. 49, pp. 35269–35277.

Allard, P., Zoubeidi, A., Nguyen, L.T., Tessier, S., Tanguay, S., Chevrette, M., Aprikian, A., *et al.* (2000), "Links between Fer tyrosine kinase expression levels and prostate cell proliferation", *Mol Cell Endocrinol*, Vol. 159 No. 1–2, pp. 63–77.

Arndt, S., Poser, I., Moser, M. and Bosserhoff, A.K. (2007), "Fussel-15, a novel Ski/Sno homolog protein, antagonizes BMP signaling", *Mol Cell Neurosci*, Vol. 34 No. 4, pp. 603–611.

Arndt, S., Schmidt, J., Wacker, E., Karrer, S. and Bosserhoff, A.-K. (2011), "Fussel-15, a New Player in Wound Healing, Is Deregulated in Keloid and Localized Scleroderma", *The American Journal of Pathology*, Vol. 178 No. 6, pp. 2622–2631.

Arregui, C., Pathre, P., Lilien, J. and Balsamo, J. (2000), "The nonreceptor tyrosine kinase fer mediates cross-talk between N-cadherin and beta1-integrins", *J Cell Biol*, Vol. 149 No. 6, pp. 1263–1274.

Aversa, C., Rossi, V., Geuna, E., Martinello, R., Milani, A., Redana, S., Valabrega, G., *et al.* (2014), "Metastatic breast cancer subtypes and central nervous system metastases", *The Breast*, Vol. 23 No. 5, pp. 623–628.

Bishop, A.C., Kung, C., Shah, K., Witucki, L., Shokat, K.M. and Liu, Y. (1999), "Generation of Monospecific Nanomolar Tyrosine Kinase Inhibitors via a Chemical Genetic Approach", *Journal of the American Chemical Society*, Vol. 121 No. 4, pp. 627–631.

Bishop, A.C., Ubersax, J.A., Petsch, D.T., Matheos, D.P., Gray, N.S., Blethrow, J., Shimizu, E., *et al.* (2000), "A chemical switch for inhibitor-sensitive alleles of any protein kinase", *Nature*, Vol. 407 No. 6802, pp. 395–401.

Borten, M.A., Bajikar, S.S., Sasaki, N., Clevers, H. and Janes, K.A. (2018), "Automated brightfield morphometry of 3D organoid populations by OrganoSeg", *Scientific Reports*, Vol. 8 No. 1, p. 5319.

Bottomley, M.J., Collard, M.W., Huggenvik, J.I., Liu, Z., Gibson, T.J. and Sattler, M. (2001), "The SAND domain structure defines a novel DNA-binding fold in transcriptional regulation", *Nature Structural Biology*, Vol. 8 No. 7, pp. 626–633.

Chazaud, B., Ricoux, R., Christov, C., Plonquet, A., Gherardi, R.K. and Barlovatz-Meimon, G. (2002), "Promigratory Effect of Plasminogen Activator Inhibitor-1 on Invasive Breast Cancer Cell Populations", *The American Journal of Pathology*, Vol. 160 No. 1, pp. 237–246.

Chen, Y.-G. (2009), "Endocytic regulation of TGF-β signaling", *Cell Research*, Vol. 19 No. 1, pp. 58–70.

Craig, A.W. and Greer, P.A. (2002), "Fer kinase is required for sustained p38 kinase activation and maximal chemotaxis of activated mast cells", *Mol Cell Biol*, Vol. 22 No. 18, pp. 6363–6374.

Dennler, S., Itoh, S., Vivien, D., Dijke, P. ten, Huet, S. and Gauthier, J. (1998), "Direct binding of Smad3 and Smad4 to critical TGFβ-inducible elements in the promoter of human plasminogen activator inhibitor-type 1 gene", *The EMBO Journal*, Vol. 17 No. 11, pp. 3091–3100.

Fischer, S., Bayersdorfer, F., Harant, E., Reng, R., Arndt, S., Bosserhoff, A.-K. and Schneuwly, S. (2012), "fussel (fuss) - A Negative Regulator of BMP Signaling in Drosophila melanogaster", *PLoS ONE*, Vol. 7 No. 8, p. e42349.

Gray, R., Bradley, R., Braybrooke, J., Liu, Z., Peto, R., Davies, L., Dodwell, D., *et al.* (2019), "Increasing the dose intensity of chemotherapy by more frequent administration or sequential scheduling: a patient-level meta-analysis of 37 298 women with early breast cancer in 26 randomised trials", *The Lancet*, Vol. 393 No. 10179, pp. 1440–1452.

Greer, P. (2002), "Closing in on the biological functions of Fps/Fes and Fer", *Nat Rev Mol Cell Biol*, Vol. 3 No. 4, pp. 278–289.

Guo, C. and Stark, G.R. (2011), "FER tyrosine kinase (FER) overexpression mediates resistance to quinacrine through EGF-dependent activation of NF-kappaB", *Proc Natl Acad Sci U S A*, Vol. 108 No. 19, pp. 7968–7973.

Isogai, C., Laug, W.E., Shimada, H., Declerck, P.J., Stins, M.F., Durden, D.L., Erdreich-Epstein, A., *et al.* (2001), "Plasminogen activator inhibitor-1 promotes angiogenesis by stimulating endothelial cell migration toward fibronectin.", *Cancer Research*, Vol. 61 No. 14, pp. 5587–94.

Ivanova, I.A., Arulanantham, S., Barr, K., Cepeda, M., Parkins, K.M., Hamilton, A.M., Johnston, D., *et al.* (2019), "Targeting FER Kinase Inhibits Melanoma Growth and Metastasis.", *Cancers*, Vol. 11 No. 3, p. 419.

Ivanova, I.A., Vermeulen, J.F., Ercan, C., Houthuijzen, J.M., Saig, F.A., Vlug, E.J., Wall, E. van der, *et al.* (2013), "FER kinase promotes breast cancer metastasis by regulating alpha6- and beta1-integrin-dependent cell adhesion and anoikis resistance", *Oncogene*, Vol. 32 No. 50, pp. 5582–5592.

Kapus, A., Ciano, C.D., Sun, J., Zhan, X., Kim, L., Wong, T.W. and Rotstein, O.D. (2000), "Cell volume-dependent phosphorylation of proteins of the cortical cytoskeleton and cell-cell contact sites. The role of Fyn and FER kinases.", *J Biol Chem*, Vol. 275 No. 41, pp. 32289–32298.

Kawakami, M., Morita, S., Sunohara, M., Amano, Y., Ishikawa, R., Watanabe, K., Hamano, E., *et al.* (2013), "FER overexpression is associated with poor postoperative prognosis and cancer-cell survival in non-small cell lung cancer", *Int J Clin Exp Pathol*, Vol. 6 No. 4, pp. 598–612.

Kennecke, H., Yerushalmi, R., Woods, R., Cheang, M.C.U., Voduc, D., Speers, C.H., Nielsen, T.O., *et al.* (2010), "Metastatic Behavior of Breast Cancer Subtypes", *Journal of Clinical Oncology*, Vol. 28 No. 20, pp. 3271–3277.

Kim, L. and Wong, T.W. (1995), "The cytoplasmic tyrosine kinase FER is associated with the catenin-like substrate pp120 and is activated by growth factors", *Mol Cell Biol*, Vol. 15 No. 8, pp. 4553–4561.

Kim, L. and Wong, T.W. (1998), "Growth factor-dependent phosphorylation of the actin-binding protein cortactin is mediated by the cytoplasmic tyrosine kinase FER", *J Biol Chem*, Vol. 273 No. 36, pp. 23542–23548.

Kirsch, D.G. and Loeffler, J.S. (2005), "Brain Metastases in Patients with Breast Cancer: New Horizons", *Clinical Breast Cancer*, Vol. 6 No. 2, pp. 115–124.

Ladwein, M. and Rottner, K. (2008), "On the Rho'd: The regulation of membrane protrusions by Rho-GTPases", *FEBS Letters*, Vol. 582 No. 14, pp. 2066–2074.

Li, H., Ren, Z., Kang, X., Zhang, L., Li, X., Wang, Y., Xue, T., *et al.* (2009), "Identification of tyrosine-phosphorylated proteins associated with metastasis and functional analysis of FER in human hepatocellular carcinoma cells", *BMC Cancer*, Vol. 9, p. 366.

Liu, J., Chen, Z., Huang, M., Tang, S., Wang, Q., Hu, P., Gupta, P., *et al.* (2020), "Plasminogen activator inhibitor (PAI) trap3, an exocellular peptide inhibitor of PAI-1, attenuates the rearrangement of F-actin and migration of cancer cells", *Experimental Cell Research*, Vol. 391 No. 1, p. 111987.

Luo, K. (2004), "Ski and SnoN: negative regulators of TGF-β signaling", *Current Opinion in Genetics & Development*, Vol. 14 No. 1, pp. 65–70.

Luo, K., Stroschein, S.L., Wang, W., Chen, D., Martens, E., Zhou, S. and Zhou, Q. (1999), "The Ski oncoprotein interacts with the Smad proteins to repress TGFβ signaling", *Genes & Development*, Vol. 13 No. 17, pp. 2196–2206.

Menges, C.W., Chen, Y., Mossman, B.T., Chernoff, J., Yeung, A.T. and Testa, J.R. (2010), "A Phosphotyrosine Proteomic Screen Identifies Multiple Tyrosine Kinase Signaling Pathways Aberrantly Activated in Malignant Mesothelioma", *Genes Cancer*, Vol. 1 No. 5, pp. 493–505.

Mizuhara, E., Nakatani, T., Minaki, Y., Sakamoto, Y. and Ono, Y. (2005), "Corl1, a Novel Neuronal Lineage-specific Transcriptional Corepressor for the Homeodomain Transcription Factor Lbx1*", *Journal of Biological Chemistry*, Vol. 280 No. 5, pp. 3645–3655.

Nawshad, A., LaGamba, D., Polad, A. and Hay, E.D. (2005), "Transforming Growth Factor-β Signaling during Epithelial-Mesenchymal Transformation: Implications for Embryogenesis and Tumor Metastasis", *Cells Tissues Organs*, Vol. 179 No. 1–2, pp. 11–23.

Nicol, R. and Stavnezer, E. (1998), "Transcriptional Repression by v-Ski and c-Ski Mediated by a Specific DNA Binding Site*", *Journal of Biological Chemistry*, Vol. 273 No. 6, pp. 3588–3597.

Nicol, R., Zheng, G., Sutrave, P., Foster, D.N. and Stavnezer, E. (1999), "Association of specific DNA binding and transcriptional repression with the transforming and myogenic activities of c-Ski.", *Cell Growth & Differentiation : The Molecular Biology Journal of the American Association for Cancer Research*, Vol. 10 No. 4, pp. 243–54.

Oshi, M., Okano, M., Maiti, A., Rashid, O.M., Saito, K., Kono, K., Matsuyama, R., *et al.* (2020), "Novel Breast Cancer Brain Metastasis Patient-Derived Orthotopic Xenograft Model for Preclinical Studies", *Cancers*, Vol. 12 No. 2, p. 444.

Pasder, O., Shpungin, S., Salem, Y., Makovsky, A., Vilchick, S., Michaeli, S., Malovani, H., *et al.* (2006), "Downregulation of Fer induces PP1 activation and cell-cycle arrest in malignant cells.", *Oncogene*, Vol. 25 No. 30, pp. 4194–4206.

Petersen, M., Pardali, E., Horst, G. van der, Cheung, H., Hoogen, C. van den, Pluijm, G. van der and Dijke, P. ten. (2010), "Smad2 and Smad3 have opposing roles in breast cancer bone metastasis by differentially affecting tumor angiogenesis", *Oncogene*, Vol. 29 No. 9, pp. 1351–1361.

Rass, M., Gizler, L., Bayersdorfer, F., Irlbeck, C., Schramm, M. and Schneuwly, S. (2022), "The Drosophila functional Smad suppressing element fuss, a homologue of the human Skor genes, retains pro-oncogenic properties of the Ski/Sno family", *PLoS ONE*, Vol. 17 No. 1, p. e0262360.

Ren, S. and Rollins, B.J. (2004), "Cyclin C/Cdk3 Promotes Rb-Dependent G0 Exit", *Cell*, Vol. 117 No. 2, pp. 239–251.

Sangrar, W., Gao, Y., Scott, M., Truesdell, P. and Greer, P.A. (2007), "Fer-mediated cortactin phosphorylation is associated with efficient fibroblast migration and is dependent on reactive oxygen species generation during integrin-mediated cell adhesion", *Mol Cell Biol*, Vol. 27 No. 17, pp. 6140–6152.

Sarayloo, F., Spiegelman, D., Rochefort, D., Akçimen, F., Oliveira, R.D.B., Dion, P.A. and Rouleau, G.A. (2020), "SKOR1 has a transcriptional regulatory role on genes involved in pathways related to restless legs syndrome", *European Journal of Human Genetics*, Vol. 28 No. 11, pp. 1520–1528.

Schackmann, R.C., Amersfoort, M. van, Haarhuis, J.H., Vlug, E.J., Halim, V.A., Roodhart, J.M., Vermaat, J.S., *et al.* (2011), "Cytosolic p120-catenin regulates growth of metastatic lobular carcinoma through Rock1-mediated anoikis resistance", *J Clin Invest*, Vol. 121 No. 8, pp. 3176–3188.

Takaesu, N.T., Stinchfield, M.J., Shimizu, K., Arase, M., Quijano, J.C., Watabe, T., Miyazono, K., *et al.* (2012), "Drosophila CORL is required for Smad2-mediated activation of Ecdysone Receptor expression in the mushroom body", *Development*, Vol. 139 No. 18, pp. 3392–3401.

Takeshima, H., Shimuta, M., Komazaki, S., Ohmi, K., Nishi, M., Iino, M., Miyata, A., *et al.* (1998), "Mitsugumin29, a novel synaptophysin family member from the triad junction in skeletal muscle", *Biochemical Journal*, Vol. 331 No. 1, pp. 317–322.

Tavares, S., Liv, N., Pasolli, M., Opdam, M., Rätze, M.A.K., Saornil, M., Sluimer, L.M., *et al.* (2022), "FER regulates endosomal recycling and is a predictor for adjuvant taxane benefit in breast cancer", *Cell Reports*, Vol. 39 No. 1, p. 110584.

Tecalco-Cruz, A.C., Ríos-López, D.G., Vázquez-Victorio, G., Rosales-Alvarez, R.E. and Macías-Silva, M. (2018), "Transcriptional cofactors Ski and SnoN are major regulators of the TGF-β/Smad signaling pathway in health and disease", *Signal Transduction and Targeted Therapy*, Vol. 3 No. 1, p. 15.

Teo, K., Gómez-Cuadrado, L., Tenhagen, M., Byron, A., Rätze, M., Amersfoort, M. van, Renes, J., *et al.* (2018), "E-cadherin loss induces targetable autocrine activation of growth factor signalling in lobular breast cancer", *Scientific Reports*, Vol. 8 No. 1, p. 15454.

Tinevez, J.-Y., Perry, N., Schindelin, J., Hoopes, G.M., Reynolds, G.D., Laplantine, E., Bednarek, S.Y., *et al.* (2017), "TrackMate: An open and extensible platform for single-particle tracking", *Methods*, Vol. 115, pp. 80–90.

Ven, R.A.H. van de, Tenhagen, M., Meuleman, W., Riel, J.J.G. van, Schackmann, R.C.J. and Derksen, P.W.B. (2015), "Nuclear p120-catenin regulates the anoikis resistance of mouse lobular breast cancer cells through Kaiso-dependent Wnt11 expression", *Disease Models & Mechanisms*, Vol. 8 No. 4, pp. 373–384.

Wu, J.-W., Krawitz, A.R., Chai, J., Li, W., Zhang, F., Luo, K. and Shi, Y. (2002), "Structural Mechanism of Smad4 Recognition by the Nuclear Oncoprotein Ski Insights on Ski-Mediated Repression of TGF-β Signaling", *Cell*, Vol. 111 No. 3, pp. 357–367.

Yakymovych, I., Yakymovych, M. and Heldin, C.-H. (2017), "Intracellular trafficking of transforming growth factor β receptors", *Acta Biochimica et Biophysica Sinica*, Vol. 50 No. 1, pp. 3–11.

Yoneyama, T., Angata, K., Bao, X., Courtneidge, S., Chanda, S.K. and Fukuda, M. (2012), "Fer kinase regulates cell migration through α-dystroglycan glycosylation", *Molecular Biology of the Cell*, Vol. 23 No. 5, pp. 771–780.

Yu, L., Liu, X., Cui, K., Di, Y., Xin, L., Sun, X., Zhang, W., *et al.* (2015), "SND1 Acts Downstream of TGFβ1 and Upstream of Smurf1 to Promote Breast Cancer Metastasis", *Cancer Research*, Vol. 75 No. 7, pp. 1275–1286.

Zheng, Y., Sethi, R., Mangala, L.S., Taylor, C., Goldsmith, J., Wang, M., Masuda, K., *et al.* (2018), "Tuning microtubule dynamics to enhance cancer therapy by modulating FER-mediated CRMP2 phosphorylation.", *Nature Communications*, Vol. 9 No. 1, p. 476.

Zirngibl, R., Schulze, D., Mirski, S.E., Cole, S.P. and Greer, P.A. (2001), "Subcellular localization analysis of the closely related Fps/Fes and Fer protein-tyrosine kinases suggests a distinct role for Fps/Fes in vesicular trafficking", *Exp Cell Res*, Vol. 266 No. 1, pp. 87–94.

Figures

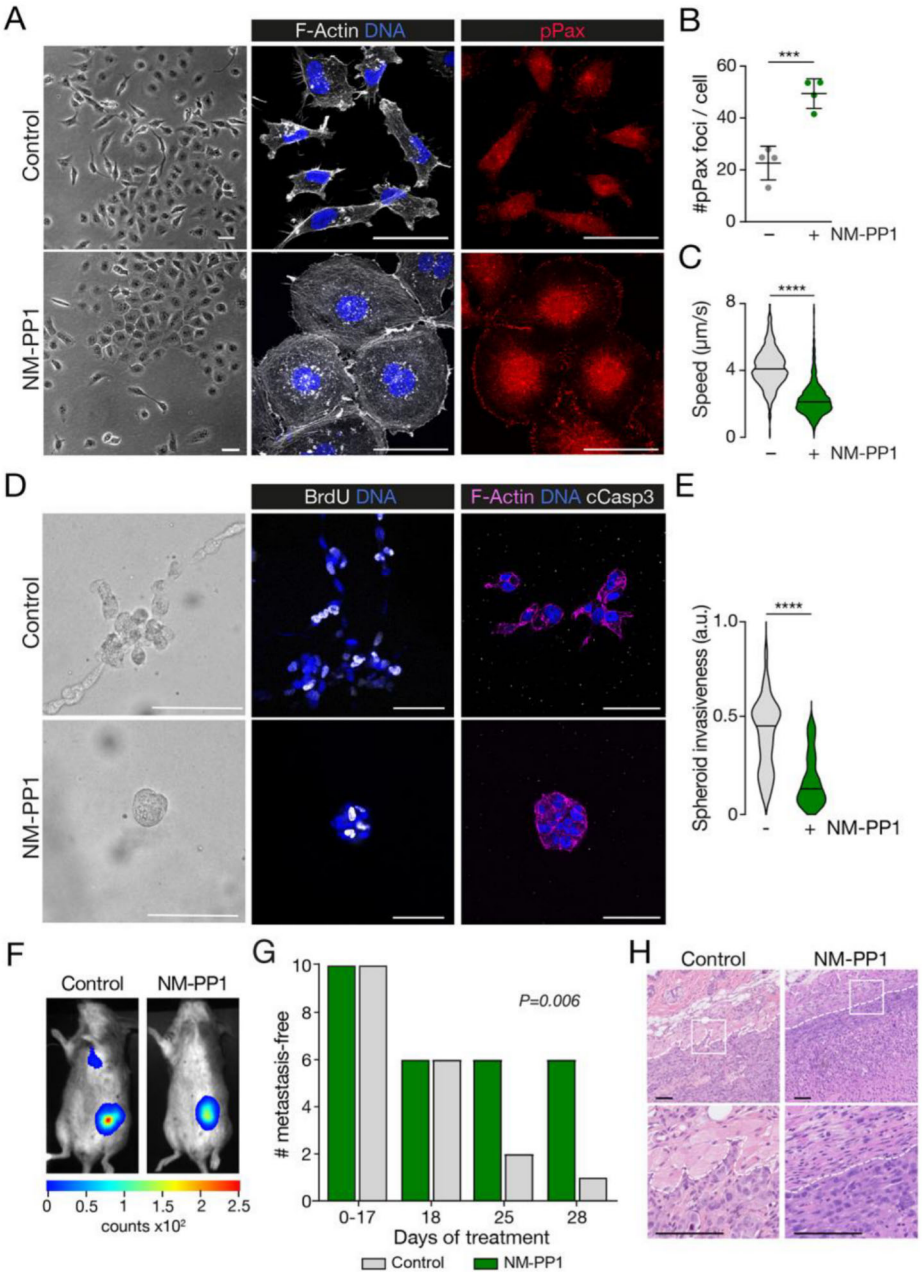

Fig. 1. FER kinase activity promotes cell migration and invasion.

A-C. Inhibition of FER-AS kinase using NM-PP1 induces cell spreading, stress fiber formation and FA formation, and reduces motility in MM231 cells. Cells were imaged by phase-contrast and stained for F-actin (middle panel, white), DNA (DAPI, middle panel, blue) and pPax (right panel, red). Scale bars, 50 µm. Quantifications of pPax foci in FER^{ASKI} cells treated with NM-PP1 (*n*=65) or without NM-PP1 (*n*=43) are shown in (B). Quantifications are from at least three independent experiments. Migration speed was quantified in (C) using live fluorescence imaging of MM231 FER^{ASKI} cells treated with control (*n*=4815) or with NM-PP1 (*n*=4171). Quantifications are from three independent experiments. **D-E.** FER kinase is

essential for 3D invasion. FER^{ASKI} cells were plated in BME as tumor spheroids, treated with NM-PP1 and imaged by phase-contrast and stained for BrdU incorporation (middle panel, white), cleaved Caspase-3 (right panel, white), F-actin (right panel, magenta) and DNA (DAPI, blue). Scale bars, 50 µm. Quantification of invasiveness of tumor spheroids treated with DMSO (*n*=36) or NM-PP1 (*n*=43) is shown in (E). Error bars denote standard deviation; * P<0.05, ** P<0.01, **** P<0.0001, ns indicates non-significant; one-way ANOVA. **F-G.** Inhibition of FER kinase activity prolongs metastasis-free survival in mice. FER^{ASKI} cells were xenografted, and tumor volume and metastasis formation were monitored upon administration of DMSO (control, *n*=10) or NM-PP1 (*n*=10). Metastasis was determined by lung bioluminescence or post-mortem assessment of lung metastatic foci. Representative images of mice treated with control or NM-PP1 at end points are shown in (F). Survival of mice upon treatment is shown in (G). Statistical analysis of survival distributions for the different treatments was performed using Log Rank (Mantel-Cox) test. **H.** FER kinase activity regulates tumor invasion. Dashed white lines indicate tumor (T)-normal (N) breast tissue border. Inset images correspond to a 200% magnification. Scale bars, 100 µm.

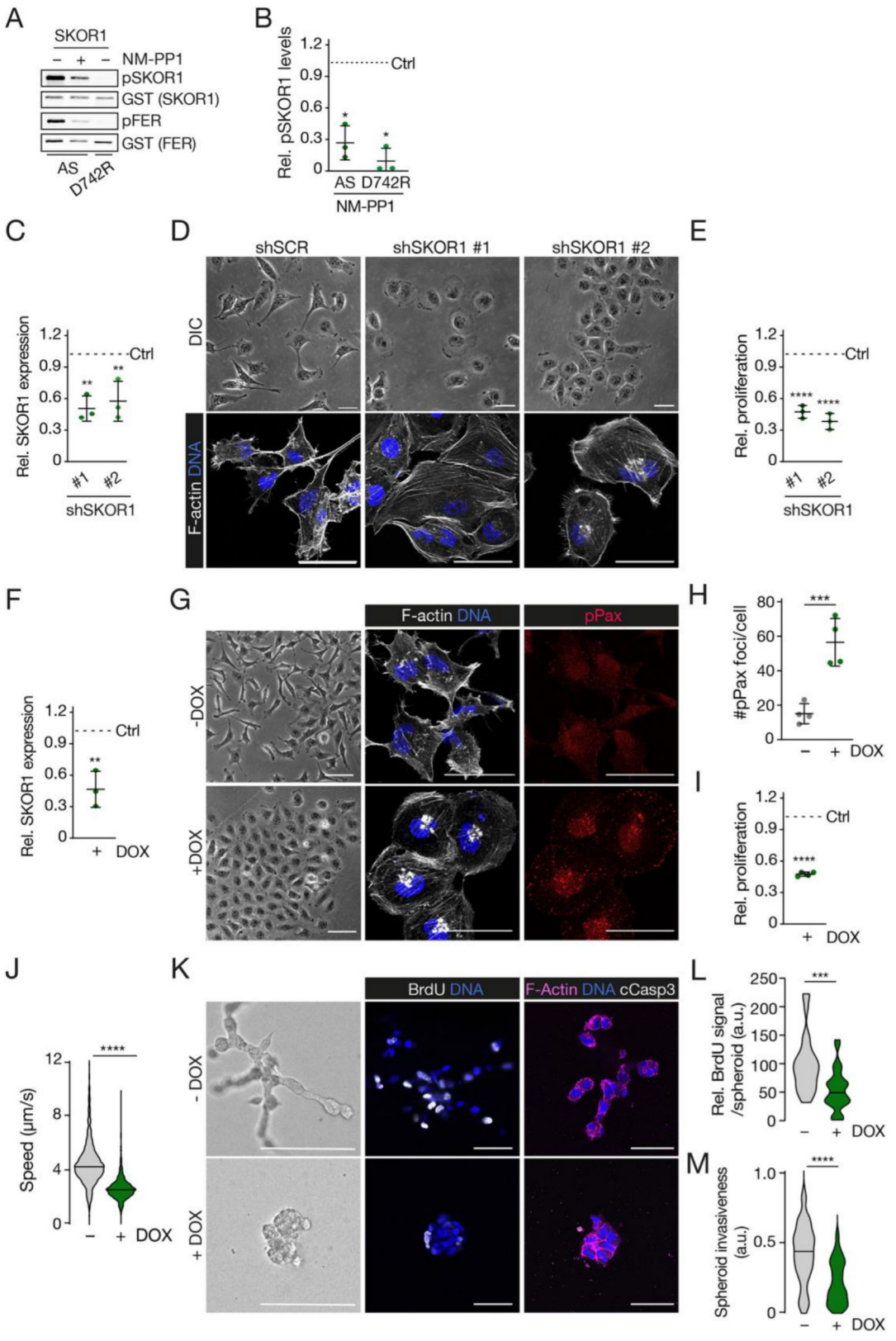

Fig. 2. SKOR1 is a FER kinase substrate that promotes breast cancer cell proliferation and invasion.

A-B. FER phosphorylates SKOR1 in vitro. Kinase assay using recombinant GST-analog sensitive FER (AS) or GST-kinase dead FER (D742R) in the presence of N-benzyl(Bn)-ATPγS, with (+) or without (-) NM-PP1.

GST-tagged SKOR1^{WT} was used as substrate. Thio-phosphorylated proteins were detected with a thiophosphate ester epitope-specific antibody. Auto-thio-phosphorylation of FER served as positive control. GST-FER was used as loading control. Depicted are the fold-changes of the thio-phosphorylated FER (AS) or GST-kinase dead FER (D742R) protein levels from at least three independent experiments compared to the control samples (Ctrl, dashed line)(B). **C-D and F-H.** SKOR1 is critical for TNBC cell morphology in 2D. Validation of SKOR1 knock-down using real-time quantitative-PCR amplification in stable (C) and DOX-inducible (F) KD cells. Relative fold-changes of SKOR1 expression compared to control samples (Ctrl, dashed line) in stable (C) and DOX-inducible (F) KD cells were quantified from three independent experiments. MM231 stable SKOR1 KD cells were imaged using phase-contrast (upper panel) and stained for F-actin (lower panel, white) and DNA (DAPI, blue) (D). MM231 SKOR1 iKD cells were treated with DOX and imaged by phase-contrast (left panel) and stained for F-actin (middle panel, white), pPax (right panel, red) and DNA (DAPI, blue) (G). Scale bars, 50 µm. Quantifications of pPax foci in SKOR iKD cells treated with (*n*=87) or without DOX (*n*=71) are shown in (H). Note the cell spreading, stress fiber formation and increase in FA formation upon SKOR1 loss. **E and I.** SKOR1 controls TNBC cell proliferation. Relative fold-changes of cell proliferation compared to control samples (Ctrl, dashed line) were quantified upon stable (E) and DOX-inducible (I) SKOR1 KD cells, using colony formation assays. **J.** SKOR1 is important for 2D cell motility. Migration speed was quantified in using live fluorescence imaging of MM231 SKOR1 iKD cells transfected with pGK-GFP, treated with (n=6136) or without DOX (n=6870) and grown in 2D. Quantifications are from three independent experiments. **K-M** SKOR1 is required for proliferation and invasion in 3D. MM231 SKOR1 iKD cells were treated with DOX and plated in BME to form 3D spheres. Cells were imaged by phase-contrast and stained for BrdU (middle panel, white), cleaved Caspase-3 (right panel, white), F-actin (right panel, magenta) and DNA (DAPI, blue). Scale bars, 50 µm. Quantification of BrdU positive nuclei of SKOR1 iKD spheroids treated with (*n*=28) or without DOX (*n*=29) is shown in (L). Quantification of spheroid invasion of SKOR1 iKD spheroids treated with (*n*=47) or without DOX (*n*=38) is shown in (M). Error bars denote s.d.; * P<0.05, ** P<0.01, **** P<0.0001, ns indicates non-significant; one-way ANOVA.

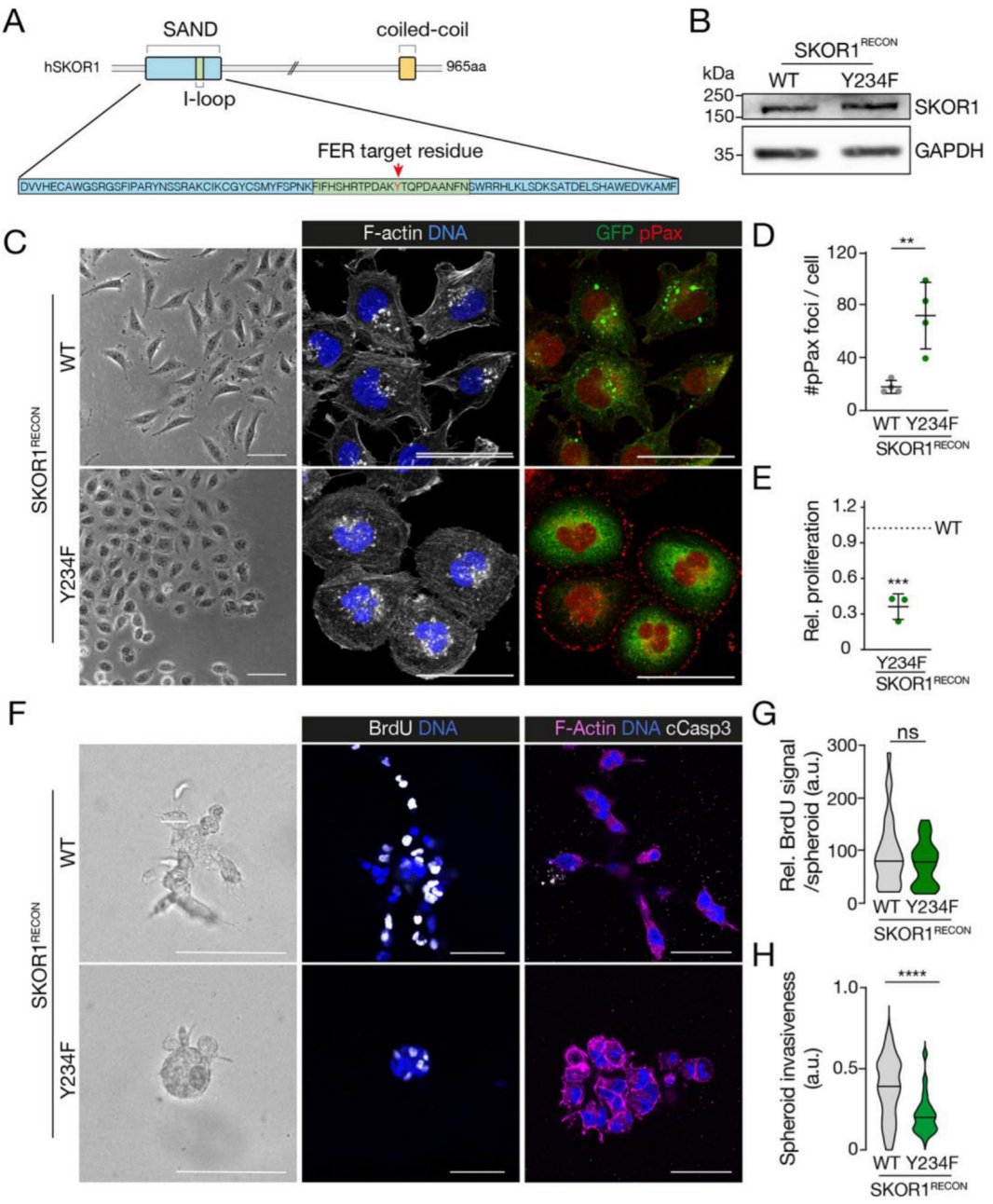

Fig. 3. SKOR1-Y234 is required for cell motility and invasion.

A. The FER target residue of SKOR1 resides in the I-loop of the SAND domain. Schematic of human SKOR1 domains. **B-H.** MM231 SKOR1 iKD cells were reconstituted ($SKOR1^{RECON}$) with either SKOR1 wild-type ($SKOR1^{WT}$) or SKOR1 mutant whereby tyrosine 234 was substituted for phenylalanine ($SKOR1^{Y234F}$). **B.** $SKOR1^{WT}$ and $SKOR1^{Y234F}$ are equally expressed. Shown are protein levels of SKOR1 in indicated cells as determined by western blotting. GAPDH was used as loading control. **C-E.** The SKOR1 Y234 residue is required for motility, invasion, and proliferation. Cells were stained for F-actin (middle panel, white), pPax (right panel, red) and DNA (DAPI, blue) (C). Scale bars, 50 µm. Note the extensive cell spreading and increase in the number of pPax foci in $SKOR1^{Y234F}$ cells. Note the cytoplasmic localization of SKOR1 in the WT and Y234F reconstituted cells (right panel). Quantifications of FA

formation in SKOR1^{WT} cells (*n*=56) or SKOR1^{Y234F} cells (*n*=63) are shown in (D). Quantifications are from three independent experiments. The relative fold-change of cell proliferation compared to control samples (Ctrl, dashed line) was quantified using colony formation assays (E). **F-H.** The Y234 residue regulates 3D invasion. SKOR1^{WT} or SKOR1^{Y234F} reconstituted cells were plated in BME as tumor spheroids. Cells were imaged by phase-contrast and stained for BrdU incorporation (middle panel, white), cleaved Caspase-3 (right panel, white), F-actin (right panel, magenta) and DNA (DAPI, blue). Scale bars, 50 µm. Quantification of BrdU positive nuclei of SKOR1^{WT} spheroids (*n*=30) or SKOR1^{Y234F} spheroids (*n*=29) is shown in (G). Quantification of spheroid invasion of SKOR1^{WT} spheroids (*n*=44) or SKOR1^{Y234F} spheroids (*n*=47) is shown in (H). Error bars denote s.d.; * P<0.05, ** P<0.01, **** P<0.0001, ns indicates non-significant; one-way ANOVA.

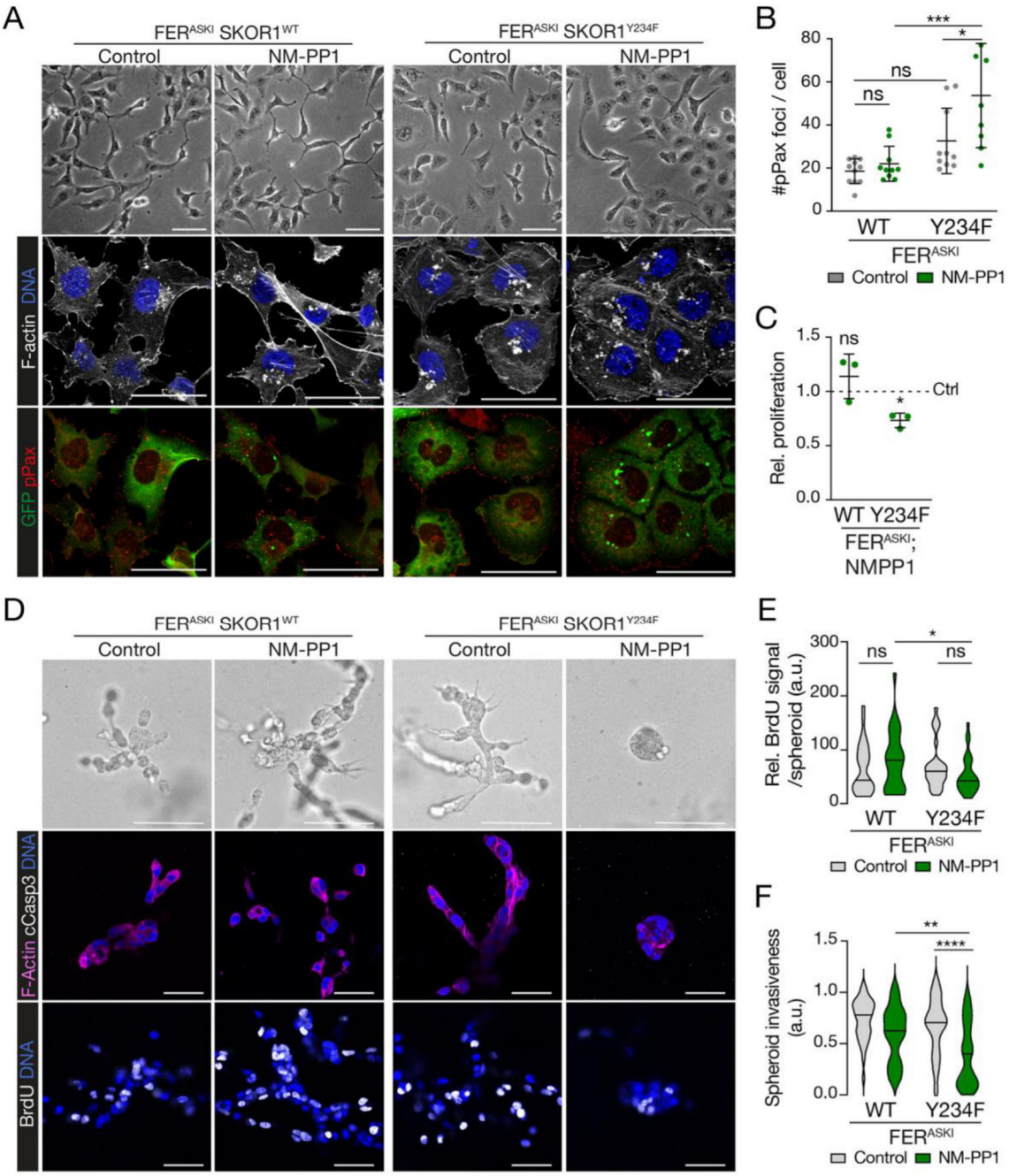

Fig. 4. SKOR1 promotes FER-induced migration and invasion through its Tyrosine 234 residue.

A-C. SKOR1-Y234 controls FER-induced cell motility and proliferation. MM231 FER^{ASKI} cells expressing SKOR1^{WT} or SKOR1^{Y234F} (green) were imaged by phase-contrast and stained for F-actin (middle panel, white), pPax (lower panel, red) and DNA (DAPI). Scale bars, 50 µm. Quantifications of pPax foci in FER^{ASKI} cells expressing SKOR1^{WT} treated with DMSO (*n*=129) or NMPP1 (*n*=163), or SKOR1^{Y234F} treated with DMSO (*n*=151) or NMPP1 (*n*=121) are shown in (B). Quantifications are from three independent experiments. The relative fold-change of cell proliferation compared to control samples (dashed line) was quantified using colony formation assays (C). **D-F.** SKOR1-Y234 is critical for FER-induced 3D invasion. MM231 FER^{ASKI} cells expressing SKOR1^{WT} or SKOR1^{Y234F} (green) were cultured in the presence

of NM-PP1 and plated in BME as tumor spheroids. Cells were imaged by phase-contrast and stained for BrdU incorporation (middle panel, white), cleaved Caspase-3 (right panel, white), F-actin (right panel, magenta) and DNA (DAPI, blue). Scale bars, 50 µm. Quantification of BrdU positive nuclei of FER^{ASKI} spheroids expressing $SKOR1^{WT}$ treated with DMSO (*n*=30) or NMPP1 (*n*=30), or $SKOR1^{Y234F}$ treated with DMSO (*n*=30) or NMPP1 (*n*=30) is shown in (E). Quantification of spheroid invasion of FER^{ASKI} spheroids expressing $SKOR1^{WT}$ treated with DMSO (n=36) or NMPP1 (n=42), or $SKOR1^{Y234F}$ treated with DMSO (*n*=39) or NMPP1 (*n*=41) is shown in (F). Error bars denote s.d.; * P<0.05, ** P<0.01, **** P<0.0001, ns indicates non-significant; one-way ANOVA.

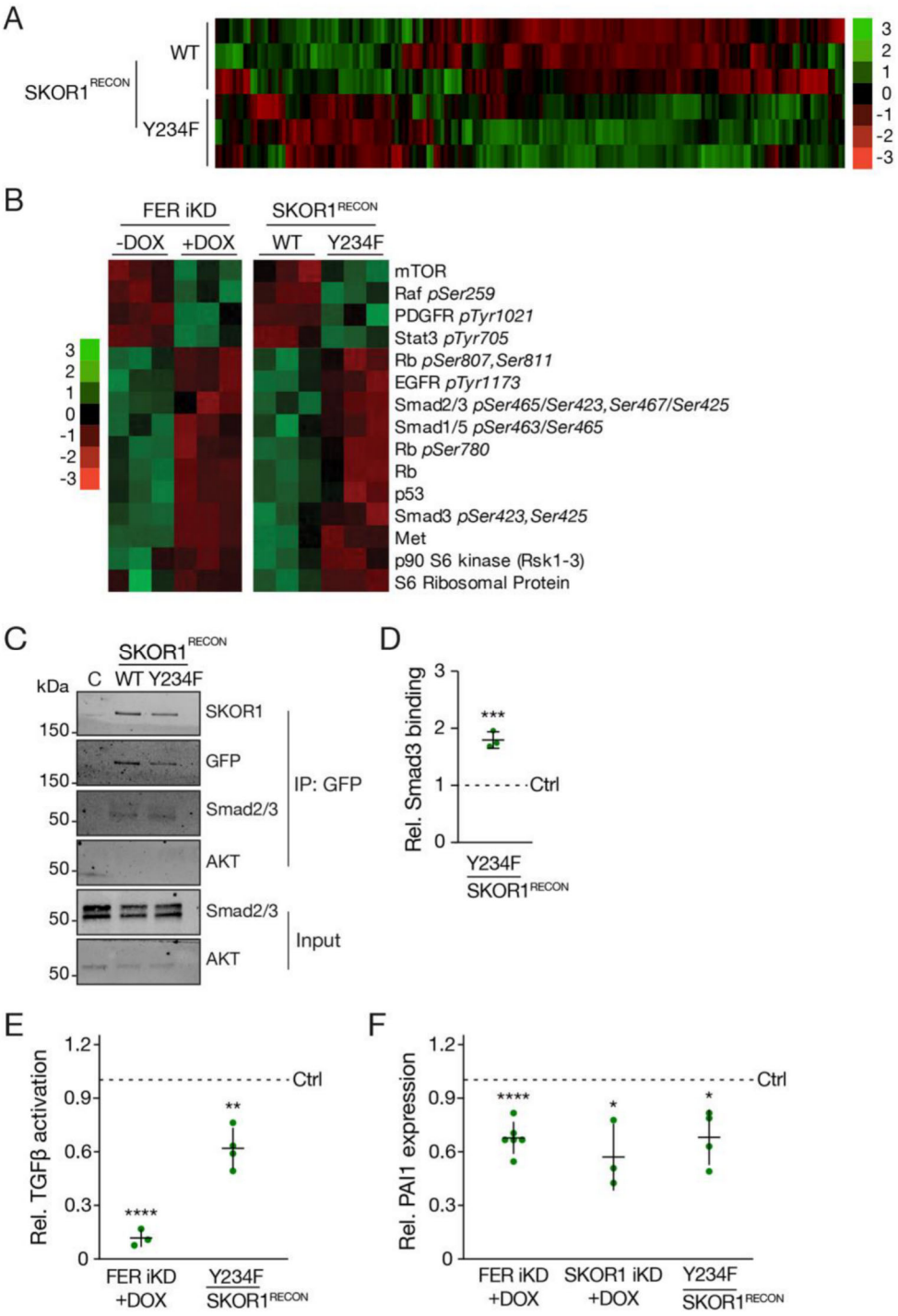

Fig. 5. FER and SKOR1-Y234 promote Smad2/3 phosphorylation.

A. SKOR1-Y234 controls multiple key signaling pathways in MM231 cells. **B.** FER and SKOR1-Y234 similarly induce phosphorylation of Smad2/3 and other key growth signaling effectors. (A and B) Heatmaps representing altered levels of phosphorylated protein residues (Z-scores). Rows represent phosphorylation sites and colors represent magnitude of intensity. The red-to-green scale indicates signal intensity. **C-D.** The SKOR1 Y234 residue controls SKOR1 binding to Smad3. Smad2/3 binding to SKOR1 was assessed in MM231 SKOR1^{RECON} cells using co-immunoprecipitation (IP) for GFP and western

blotting. A parental MM231 cell lysate was used as non-specific IP control. Shown are protein levels of Smad2/3 and SKOR1. Akt was used as loading control. Fold-changes of Smad2/3 levels bound to GFP-SKOR1^{WT} and GFP-SKOR1^{Y234F} were quantified relative to control input samples (shown as a dashed line) in (D). **E and F.** Phosphorylation of SKOR1-Y234 regulates SMAD3 specific activation of TGFβ-induced transcription. Relative fold-change of TGFβ/SMAD3 activation was determined upon FER depletion and SKOR1^{Y234F} reconstitution (E) in MM231 cells transfected with the TGFβ/SMAD3-inducible $(CAGA)_{12}$ luciferase transcriptional reporter construct. SKOR1 and FER regulate mRNA expression of *PAI1*, a TGFβ target gene. Relative *PAI1* expression was determined upon FER depletion, SKOR1 depletion and SKOR1^{Y234F} reconstitution (F) in MM231 cells. Relative fold-changes in (E) and (F) were quantified relative to control samples (Ctrl, dashed lines). Quantifications are from at least three independent experiments. Expression was normalized by GAPDH. Error bars denote s.d.; * P<0.05, **** P<0.0001; t-test.

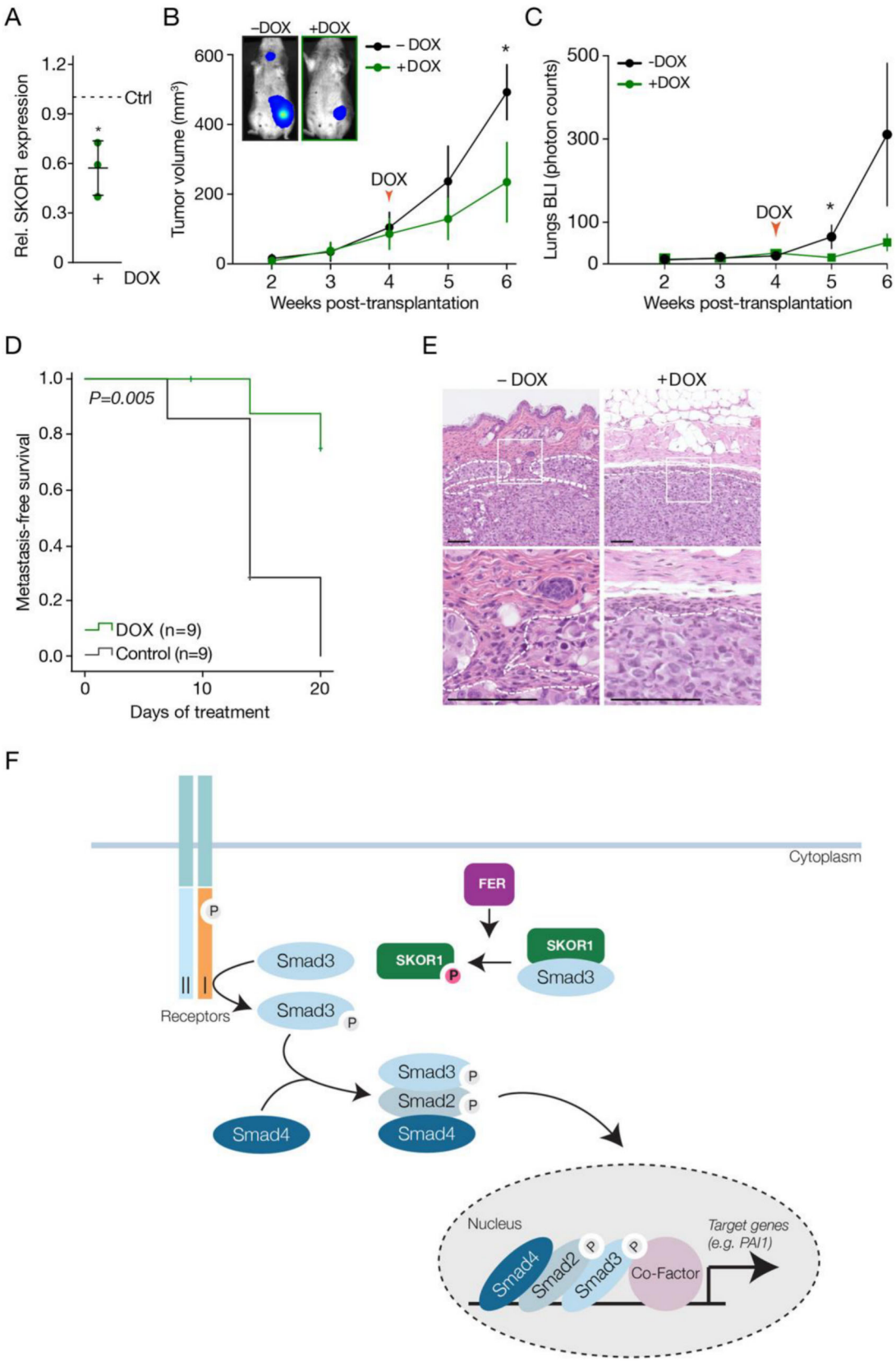

Fig. 6. SKOR1 promotes breast tumor growth and metastasis formation.

A. Validation of SKOR1 knock-down in mice breast tumors. Fold-change of SKOR1 expression relative to control samples (Ctrl, dashed line) by real-time quantitative PCR. **B-D.** SKOR1 promotes breast tumor

growth and metastasis formation in mice. Luciferase-expressing MM231 SKOR1 iKD cells were xenografted and switched to a DOX-containing diet (red arrow). upon formation of palpable tumors Primary tumor volume (B) and lung metastasis formation (C) were monitored weekly. Kaplan-Meijer analysis was used to determine cumulative survival of mice treated with (*n*=9) or without DOX (*n*=9) (D). **E.** SKOR1 promotes tumor invasion in mice. Representative H&E images of mice treated or untreated with DOX at end points. Dashed white lines indicate tumor (T)-normal (N) breast tissue border. Inset images correspond to a 200% magnification. Scale bars, 100 µm. **F.** Schematic model depicting SKOR1 as a mediator of FER-dependent Smad2/3 signaling pathways. Error bars denote s.d.; * P<0.05, ** P<0.01, **** P<0.0001, ns indicates non-significant; one-way ANOVA.

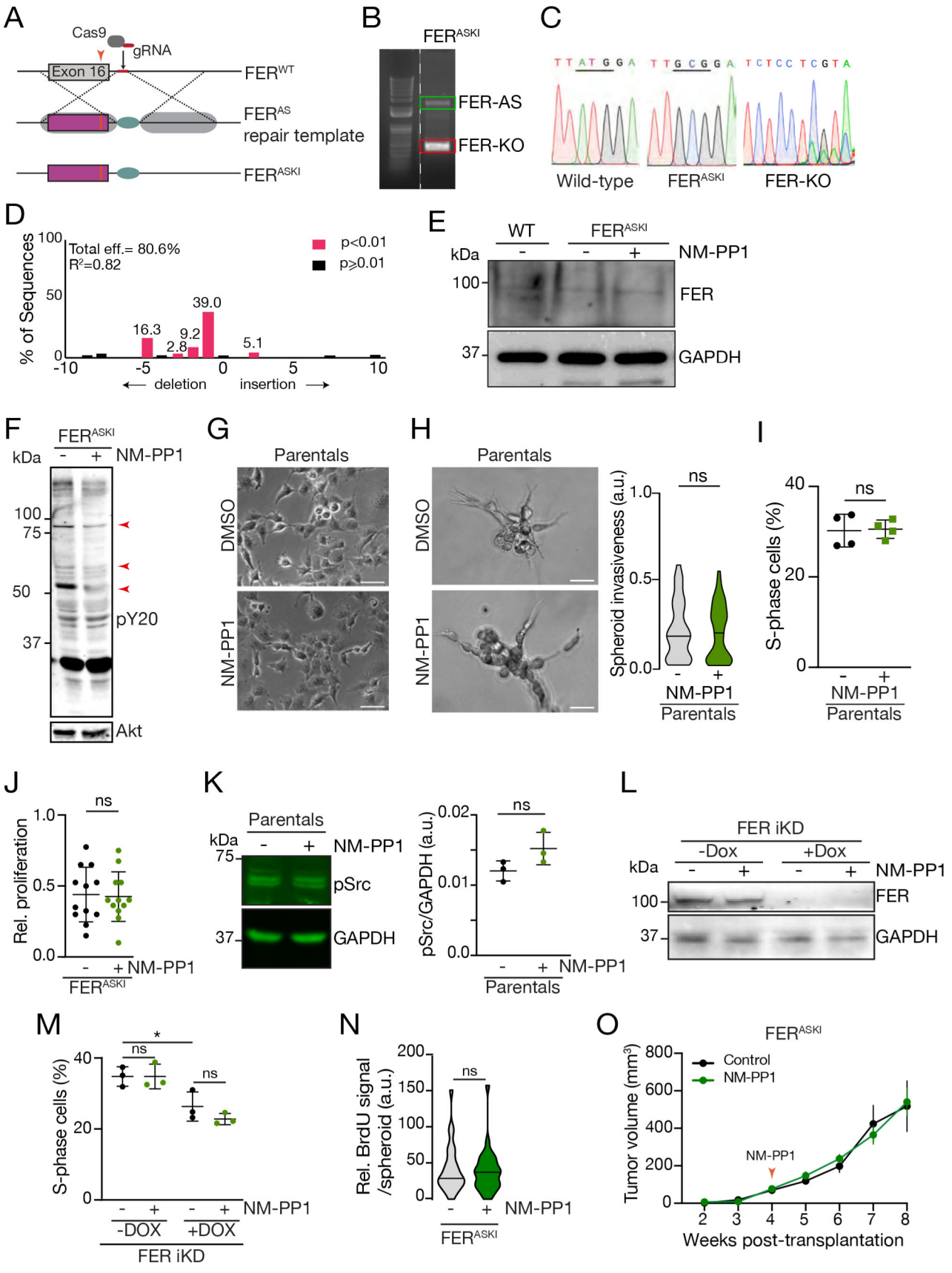

Fig. S1. Generation and validation of FER^{ASKI} cells.

A. CRISPR-Cas9 gene editing strategy generating endogenous analogue-sensitive FER expression (FER^{ASKI}). Gatekeeper residue M637 (arrow) is mutated to alanine (indicated by red line within magenta box). The repair template contains a puromycin selection cassette (turquoise). **B-D.** FER^{ASKI} cells only express gatekeeper-mutated FER kinase. *FER* alleles of FER^{ASKI} cells were PCR-amplified (B) and sequenced (C). *FER*-AS and *FER*-KO alleles were compared to MM231 parentals (wild-type). TIDE analysis of *FER*-KO is shown in (D). **E.** Protein expression of FER-AS by FER^{ASKI} cells is similar to FER-WT expression in MM231 parental cells, as determined by western blotting. GAPDH was used as loading control. **F.** Inhibiting FER kinase activity reduces phosphorylation of several tyrosine phosphorylated proteins. Shown are protein levels of phospho-tyrosine residues (pY20) in FER^{ASKI} cells treated with or without NM-PP1 as determined by western blotting. Red arrowheads depict reduced phospho-tyrosine residues upon NM-PP1 treatment. Akt was used as loading control. **G.** MM231 parental cells were treated with DMSO (control) or NM-PP1 and were imaged by phase-contrast. Scale bars, 50 µm. **H.** Parental MM231 cells were plated in Matrigel as tumor spheroids, treated with NM-PP1 and imaged by phase-contrast. Scale bars, 50 µm. Quantification of invasiveness of tumor spheroid treated with DMSO (n=44) or NM-PP1 (n=46) is shown. Error bars denote s.d.; * P<0.05, ** P<0.01, **** P<0.0001, ns indicates non-significant; one-way ANOVA. **I.** NM-PP1 treatment does not induce unspecific effects on MM231 cells proliferation. MM231 parental cells treated with or without NM-PP1 were used for cell cycle profiling, and the percentages of cells in S-phase were determined. Quantifications are based on at least three biological replicates. **J.** Cell proliferation is independent of FER kinase activity. Colony formation assays were performed using FER^{ASKI} cells and quantified. **K and L.** NM-PP1 treatment does neither affect FER protein levels in FER iKD cells treated with or without DOX nor Src activation in parental MM231 cells. FER and phospho-Src protein levels were evaluated by western blotting. GAPDH was used as loading control. Phospho-Src quantifications are from three independent experiments. **M.** NM-PP1 treatment does not induce unspecific effects on FER-depleted cells proliferation. MM231 FER iKD cell treated with or without DOX, and with or without NM-PP1 were used for cell cycle profiling, and the percentages of cells in S-phase were determined. Quantifications are from at least three biological replicates. **N.** FER^{ASKI} cells were plated in BME as tumor spheroids, treated with NM-PP1 and stained for BrdU incorporation. Quantification of BrdU positive nuclei in tumor spheroids treated with DMSO (n=26) or NM-PP1 (n=27) is shown in (I). **O.** FER kinase activity is not essential for primary tumor growth. FER^{ASKI} cells were xenografted, mice were treated with NM-PP1, after tumors reached a volume of approximately 100 mm^3, and tumor volumes were assessed weekly. Error bars denote s.d.; ns indicates non-significant; one-way ANOVA.

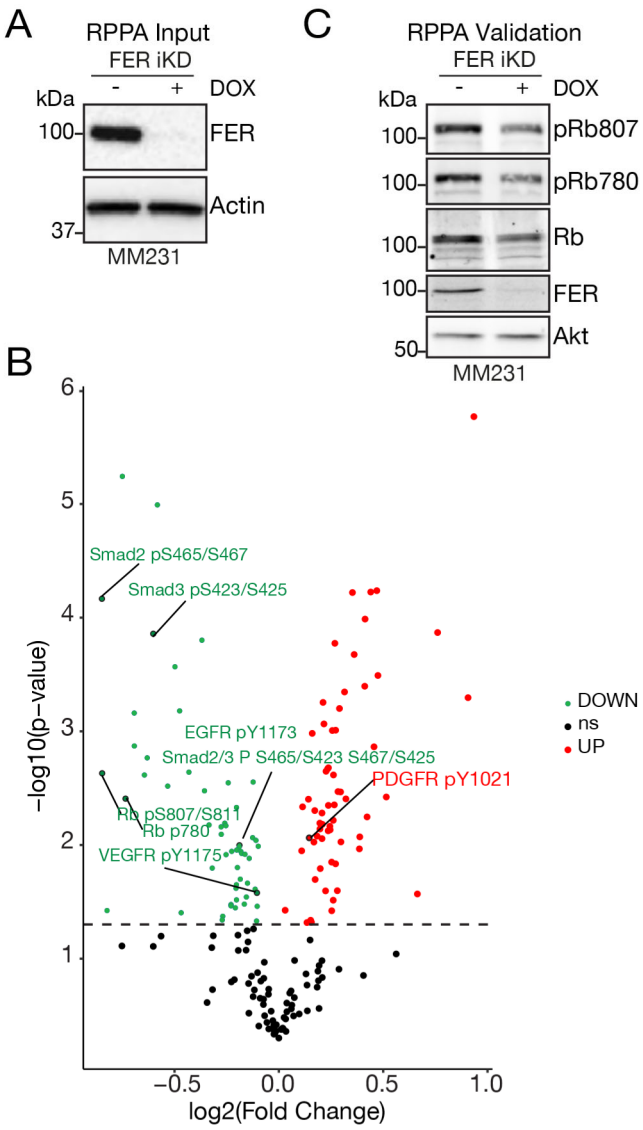

Fig. S2. FER regulates key signaling pathways in MM231 breast cancer cell line.

A. Verification of FER protein levels in MM231 FER iKD cells treated with and without DOX and used for RPPA analysis. Actin was used as loading control. **B.** Differential signaling activity in control versus FER-depleted cells. Volcano plot depicting proteins and phosphoproteins according to the average ratio of three technical replicates and p value (− log10 p value). Black points represent unchanged proteins (ns), red and green represent the upregulated and downregulated proteins respectively. Highlighted with a black border are some growth signaling effectors. The horizontal dashed line indicates p value = 0.05. **C**. Validation of RPPA data. Shown are protein levels of RPPA hits, pRb807, pRb780 and Rb, in indicated cells as determined by western blotting. Akt was used as loading control.

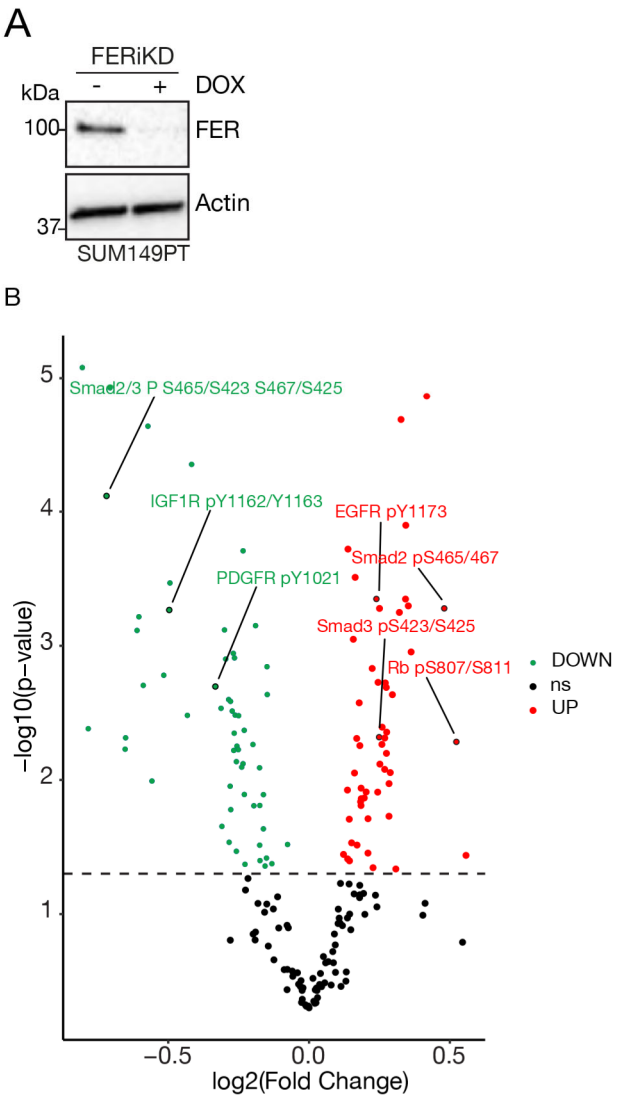

Fig. S3. FER regulates key signaling pathways in SUM149PT breast cancer cell line.

A. Verification of FER protein levels in SUM149PT FER iKD cells treated with and without DOX and used for RPPA analysis. Actin was used as loading control. **B.** Differential activity of signaling in control versus FER-depleted cells. Volcano plot depicting proteins and phosphoproteins according to the average ratio of three technical replicates and p value (− log10 p value). Black points represent unchanged proteins (ns), red and green represent the upregulated and downregulated proteins respectively. Highlighted with a black border are some growth signaling effectors. The horizontal dashed line indicates p value = 0.05.

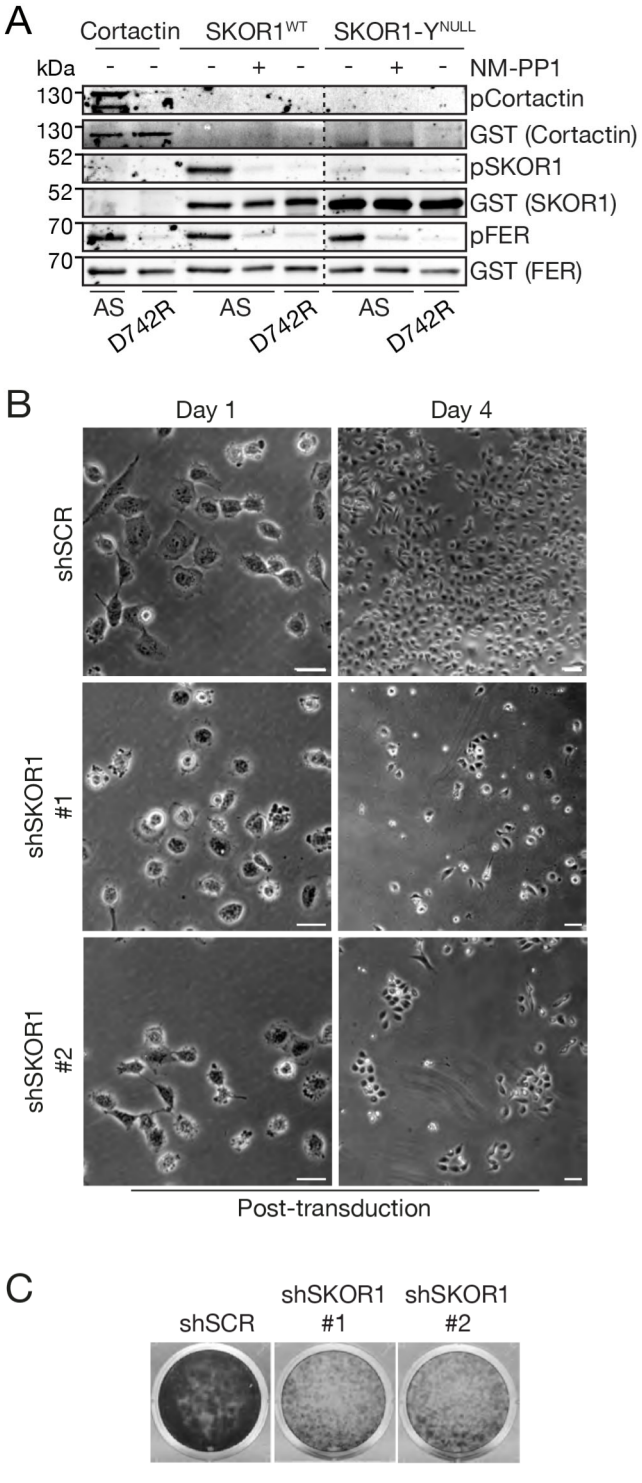

Fig. S4. SKOR1 is necessary for proliferation of MM231 breast cancer cells.

A. FER-dependent phosphorylation on SKOR1 occurs on tyrosine residues. Kinase assay using recombinant GST-analog sensitive FER (AS) or GST-kinase dead FER (D742R) in the presence of N-benzyl(Bn)-ATPγS, with (+) or without (-) NM-PP1. GST-tagged SKOR1^{WT}, GST-SKOR1-Y^{NULL} and GST-Cortactin were used as substrates. Thiophosphorylated proteins were detected with a thiophosphate ester epitope-specific antibody. Auto-thio-phosphorylation of FER and thio-phosphorylation of Cortactin served as positive controls. GST-FER was used as loading control. Dashed lines highlight non-consecutive lanes. **B-C.** MM231 cells were transduced with the indicated shRNA and imaged by phase-contrast at day 1 and day 4 following transduction. Scale bars, 50 μm (B). Following selection, colony formation was assessed in stable SKOR1 KD cells (C).

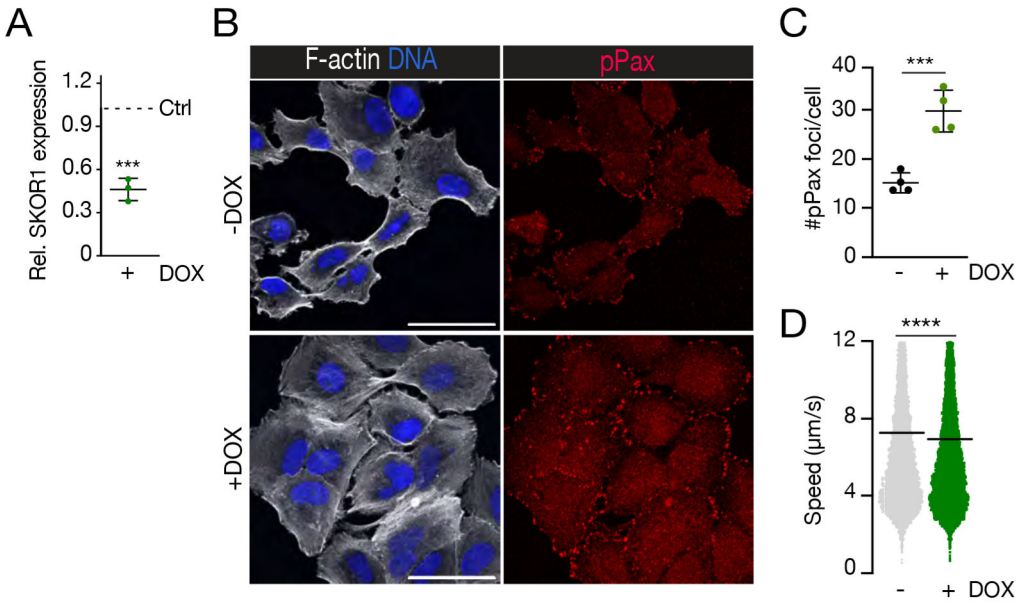

Fig. S5. SKOR1 controls focal adhesion dynamics and migration of SUM149PT cells. A. Relative fold-changes of SKOR1 expression compared to control samples (Ctrl, dashed line) in DOX-inducible KD cells were quantified from three independent experiments. **B-C.** SUM149PT SKOR1 iKD cells were treated with DOX and stained for F-actin (left panel, white), pPax (right panel, red) and DNA (DAPI, blue) (B). Scale bars, 50 μm. Quantifications of pPax foci are shown in (C) (-DOX n=66; +DO X n=51). Note the cell spreading, stress fiber formation and increase in FA formation upon SKOR1 loss. **D.** SKOR1 is important for 2D cell motility. Migration speed was quantified using live fluorescence imaging of SUM149PT SKOR1 iKD cells -DOX (n=9016) and +DOX (n=13266) grown in 2D. Error bars denote s.d.; *P<0.05, ** P<0.01, **** P<0.0001, ns indicates non-significant; one-way ANOVA.

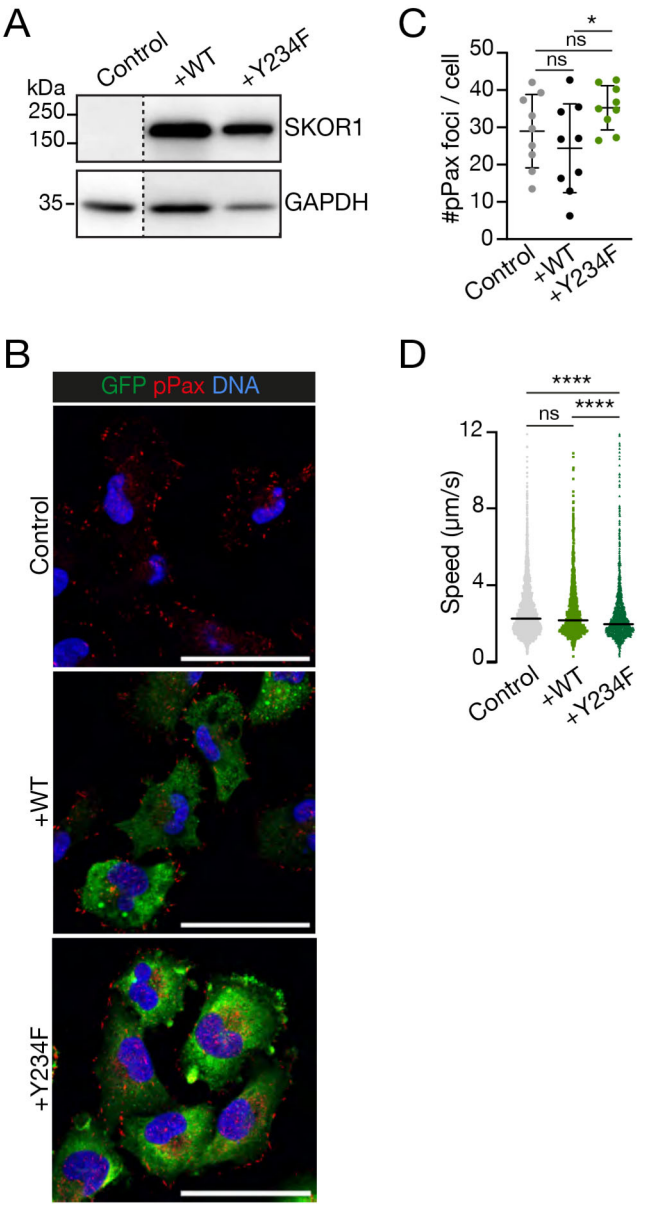

Fig. S6. Overexpression of SKOR1^{Y234F} impacts focal adhesion dynamics and migration of MM231 control cells.

A. Validation of overexpression of SKOR1^{WT} and SKOR1^{Y234F} in control cells using western blotting. Shown are protein levels of SKOR1 in untreated (control) MM231 SKOR1 iKD cells. GAPDH was used as loading control. **B-D**. SKOR1^{Y234F} overexpression impacts on focal adhesion formation and 2D cell motility. Control (left panel, *n*=108), SKOR^{WT} (middle panel, *n*=150) and SKOR1^{Y234F} cells (right panel, *n*=136) were stained for pPax (red) and DNA (DAPI, blue) (B). Scale bars, 50 µm. Quantifications of pPax foci are shown in (C). Migration speed was quantified using live fluorescence imaging of control (*n*=3340), SKOR1^{WT} (*n*=1425) and SKOR1^{Y234F} (*n*=2155) cells grown in 2D (D). Error bars denote s.d.; * P<0.05, ** P<0.01, **** P<0.0001, ns indicates non-significant; one-way ANOVA.

Figure 2A

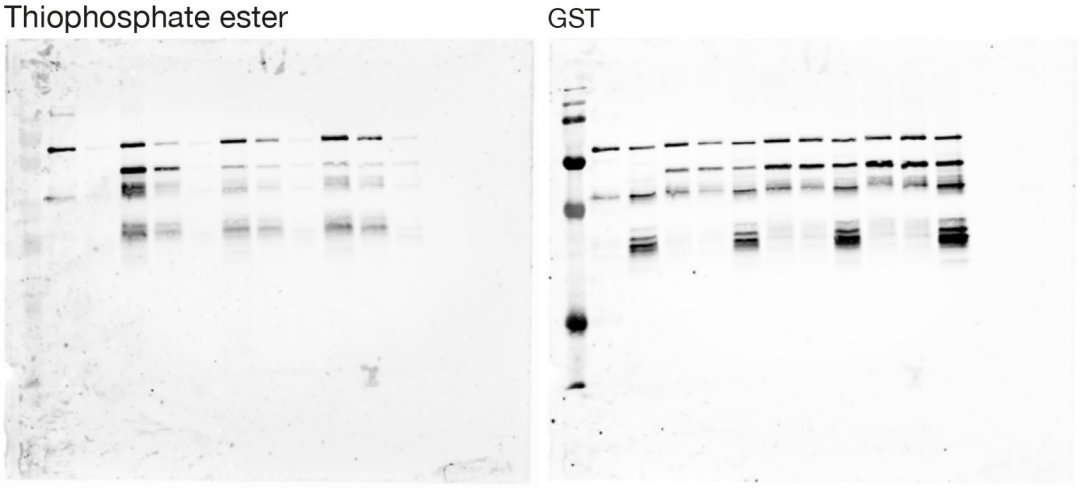

Figure 3B

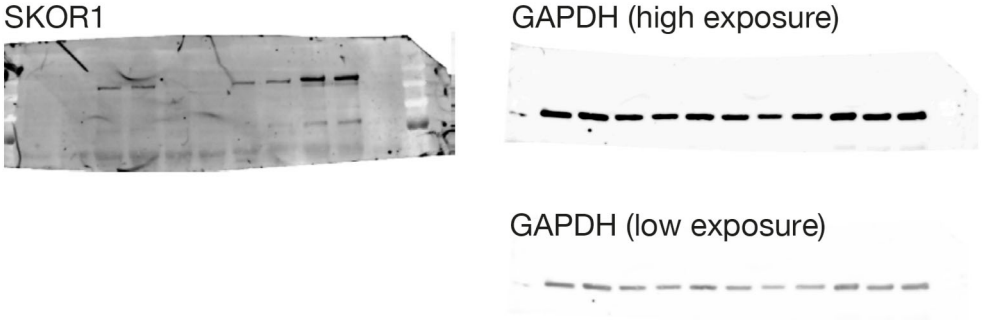

Figure 5C

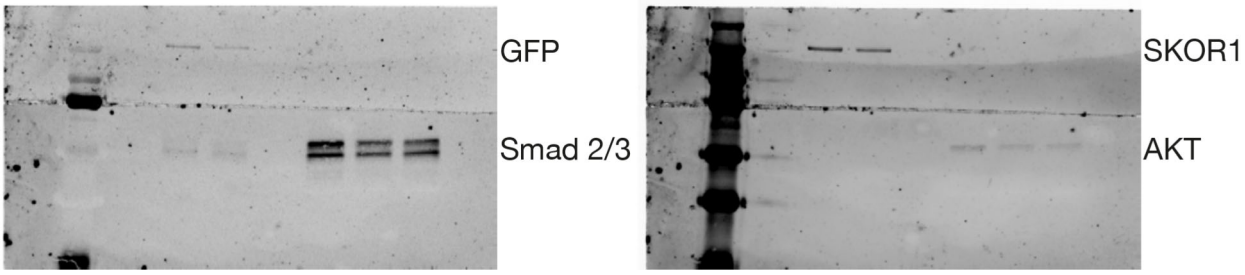

Figure S1E

FER

GAPDH

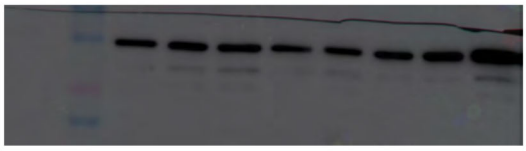

Figure S1F

pY20

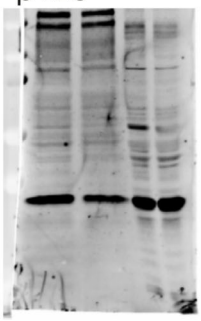

AKT

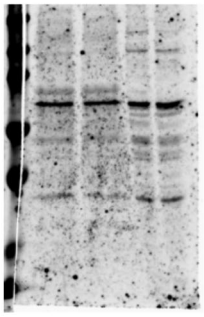

Figure S1M

FER

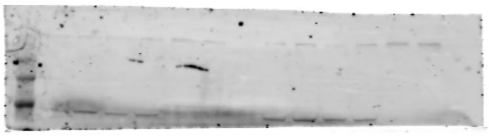

GAPDH

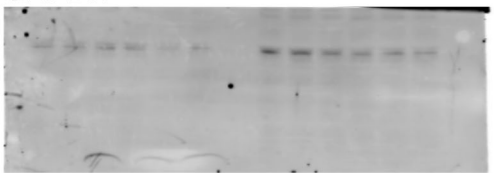

Figure S1N

pSrc

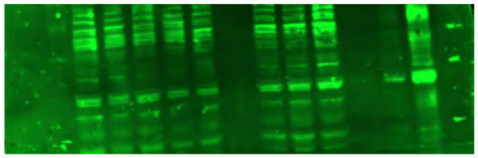

GAPDH

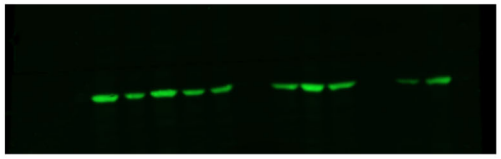

Figure S2A and S3A

FER

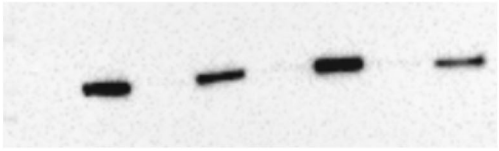

Actin

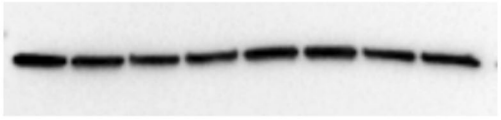

Figure S2C

FER

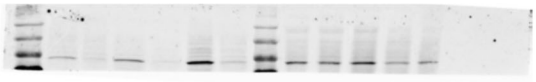

AKT

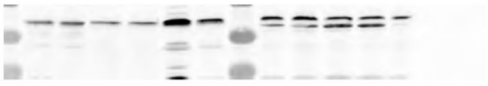

pRb p780

pRb p807

Rb

Figure S4A

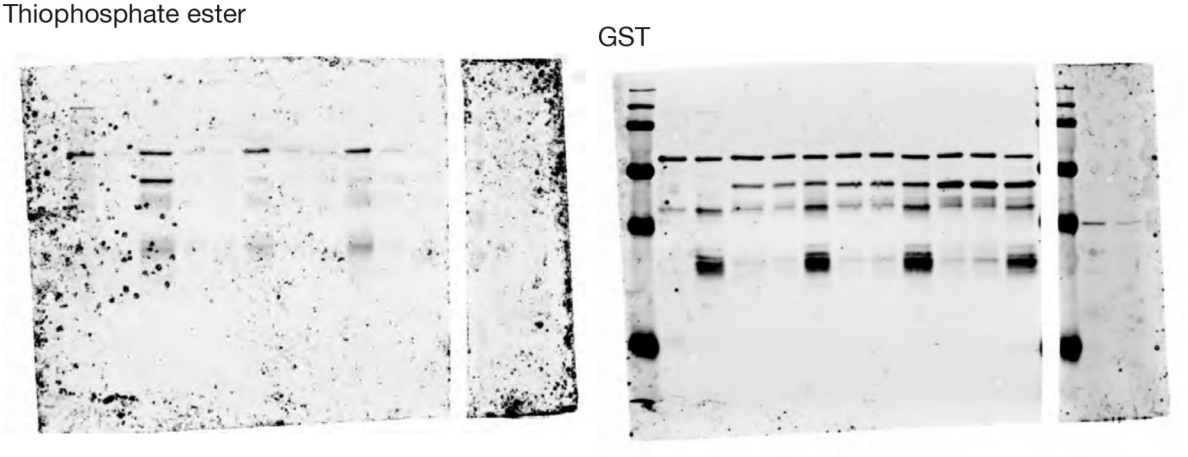

Figure S6A

Blot Transparency Figure 5C replicates

Figure 5C - replicate #2

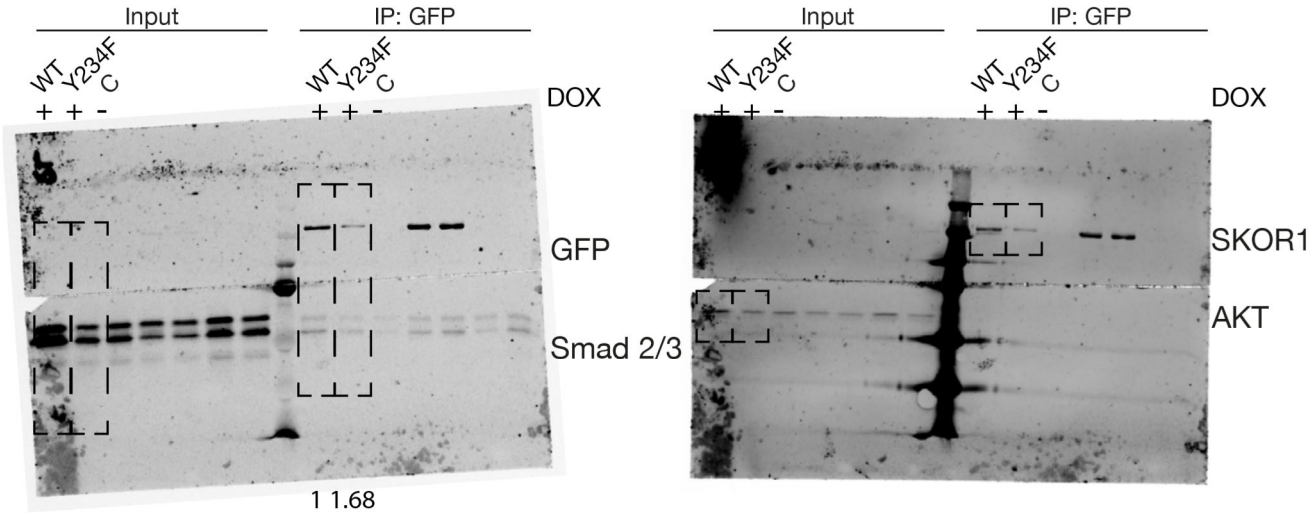

Figure 5C - replicate #3

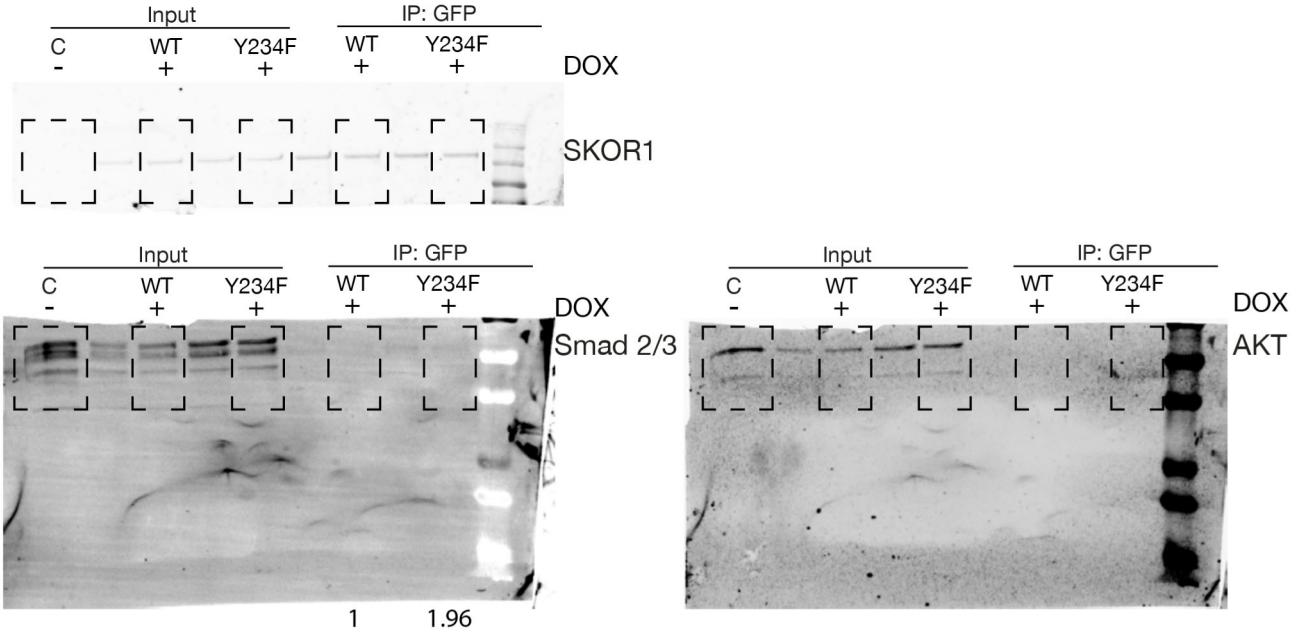

Figure S1E - replicate #2

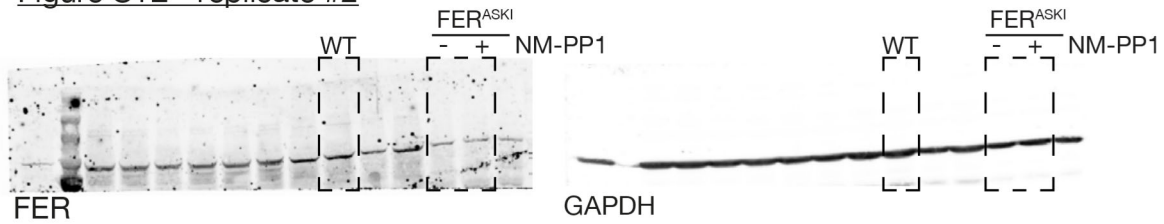

Figure S1E - replicate #3

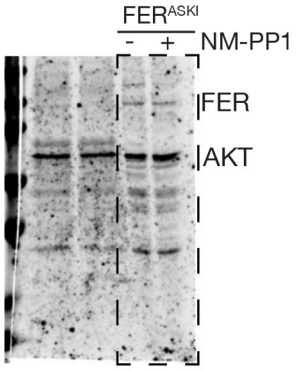

Table S1. MM231 FER iKD RPPA list of significant substrates

Click here to download Table S1

Table S2. SUM149PT FER iKD RPPA list of significant substrates

Click here to download Table S2

Table S3. MM231 SKOR1^{RECON} RPPA list of significant substrates

Click here to download Table S3